U. S. DEPARTMENT OF COMMERCE
NATIONAL OCEAN AND ATMOSPHERIC ADMINISTRATION
NATIONAL WEATHER SERVICE
NATIONAL CENTERS FOR ENVIRONMENTAL PREDICTION

OFFICE NOTE 411

ON THE SELECTION OF PROPAGATION SCHEMES FOR A SPECTRAL WIND-WAVE MODEL

HENDRIK L. TOLMAN
UCAR VISITING SCIENTIST

NOVEMBER 1995

Abstract

This report discusses the selection of accurate numerical propagation schemes for use in wind wave models. The paper utilizes previous studies in wave modeling and in the related field of pollution modeling, and does not present new numerical methods. In reviewing possible methods, it was decided to consider explicit finite difference methods only, although both implicit and semi-Lagrangian methods are potentially useful. The scheme selected for further testing is the third-order ULTIMATE QUICKEST (UQ) scheme. Using this scheme in combination with a splitting technique, the overall model will become second order accurate in both space and time. The scheme is tested for one-dimensional propagation, two-dimensional propagation of short-crested swell described by a single frequency, two-dimensional propagation of a continuous spectrum, and fetch-limited wave growth. The scheme is found to be sufficiently accurate to result in a disintegration of the wave field into discrete wave fields for common spectral discretizations. This disintegration can be avoided by introducing a diffusion tensor as suggested by Booij and Holthuijsen (1987). Contrary to conventional wisdom, common frequency resolutions of 10% are found to be insufficient to describe swell propagation accurately. The UQ scheme interacts well with source terms, resulting in accurate and stable fetch-limited growth behavior. The selected scheme shows noticeable improvements over the commonly-used first-order scheme. The most important improvements appear to be the removal of spurious maxima of south- or northward traveling waves, and an increased spatial and temporal consistency of the swell field. The latter is important for swell prediction in general, and may be important for data assimilation.

1 Introduction

Modeling wind waves on the ocean surface has been in the center of interest of engineers and scientist for more than 50 years. After the pioneering work of Gelci et al. (1956), many numerical wave models have been developed (e.g., SWAMP group, 1985; SWIM group, 1985). Such models are usually based on a balance equation for a wave energy spectrum like $F(f, \theta)$, where f and θ are

the spectral frequency and direction, respectively. Such a balance equation can be written as :

$$\frac{\partial F}{\partial t} + \nabla_x\left[\mathbf{c}_g F\right] + \frac{\partial}{\partial\theta} c_\theta F = S \; , \tag{1}$$

$$c_g = \frac{\partial\sigma}{\partial k} \; , \tag{2}$$

$$c_\theta = \frac{1}{k}\frac{\partial\sigma}{\partial d}\frac{\partial d}{\partial m} \; , \tag{3}$$

$$\sigma^2 = gk\tanh kd \; , \tag{4}$$

where d is the mean water depth, $\sigma = 2\pi f$ is the intrinsic frequency, k is the wavenumber, c_g is the group velocity (in direction θ), S is the net source term describing generation and dissipation of wave energy, $\mathbf{x}$ are general spatial coordinates and m is a coordinate perpendicular to θ. The first term of this equation describes temporal variations of the spectrum, the second term describes spatial propagation, the third term describes changes of the wave direction due to spatially varying depths (refraction) and the right side describes non-conservative processes (source terms). Note that this equation is only valid for slowly varying depths without currents. It can be expanded to include effects of slowly varying currents, without changing its basic characteristics (see, e.g., Komen et al., 1994). Similarly, it is easily modified for other definitions of the spectrum (see, e.g., Tolman, 1991).

Equation (1) is usually solved using a fractional step method (e.g., Yanenko, 1971), where separate parts of the equation are solved using consecutive partial solvers. All models known to the author treat source terms and propagation separately. It is also possible to consider the different propagation terms separately.

Over the last decades, much attention has been paid to the physical aspects of wave modeling [i.e., the right side of Eq. (1)], culminating in the development of the WAM model (WAMDIG 1988; Komen et al. 1994). This model is a third-generation wave model, which implies that a balance equation for wave energy spectra is solved directly, without prescribing a spectral shape. In this model, however, not much attention has been given to numerical methods. WAM uses first order propagation schemes, the numerical diffusion of which is usually deemed unacceptable in most fields of numerical

2

fluid mechanics. Several authors have utilized more accurate schemes (for instance, SWAMP group 1985; Neu and Won 1990; Tolman 1991, 1992), but no 'standard' has been set yet.

In the present paper the selection of an accurate propagation scheme for implementation in a third-generation wave model is discussed. The discussion and selection of schemes considers existing schemes only, and utilizes the extensive experience with numerical methods in the field of pollution and transport models, where governing equations closely resemble Eq. (1). In section 2, general methods are reviewed. Based on this review, explicit finite difference methods will be considered, although other methods, in particular implicit finite difference schemes and semi-Lagrangian methods are potentially useful. In section 3, the selection of a scheme is discussed, and the propagation properties of this scheme are tested considering propagation of swell, where the wave energy is concentrated at a single spectral frequency. The selected scheme (the third order accurate QUICKEST scheme in combination with the ULTIMATE filter) is sufficiently accurate to show effects of discrete dispersion, also known as the 'garden sprinkler effect' (Booij and Holthuijsen 1987). In section 4, solutions to this problem are discussed. In section 5, the propagation test are expanded to include continuous frequency spectra. Contrary to common belief, a frequency resolution of 10% appears insufficient to describe swell propagation accurately. Finally, the propagation scheme has to be used in combination with the source terms to represent fetch-limited growth. This combination of propagation and source terms may cause numerical problems, and is discussed in section 6. The results of this study are discussed in section 7.

2 Basic methods

For the solution of the propagation equation

$$\frac{\partial F}{\partial t} + \nabla_x \left[\mathbf{c}_g F \right] + \frac{\partial}{\partial \theta} c_\theta F = 0 \,, \tag{5}$$

three basic solution techniques are available. Standard methods are the Finite Difference (FD) and Finite Element (FE) methods. The hyperbolic character of Eq. (5) furthermore makes a characteristic or semi-Lagrangian method potentially useful.

The method of characteristics, better known in ocean wave modeling as the 'ray method' represents a classical approach to wave propagation (e.g., Whitham 1974; Mei 1983). A distinction can be made between a full ray method, where rays originate at the lateral boundaries of the area considered, or partial ray methods, where rays are traced for a given time interval. Full ray models are mainly used for steady propagation problems (without source terms) and for models predicting wave spectra at selected points. This method is particularly useful as it provides insight in, for instance, effects of variable water depths and variable currents (reviews by Peregrine and Jonsson 1983; Holthuijsen and Tolman 1991). However, the full ray method results in a scattering of information in both physical and spectral space. This is detrimental for the evaluation of source terms which require information of the entire spectrum (whitecapping and nonlinear interactions). For this reason full ray methods are generally not deemed suitable for third-generation wave models. Partial ray methods or semi-Lagrangian methods do not have this deficiency. They furthermore can be made unconditionally stable, allowing for large time steps. The treatment of boundary conditions, however, particularly considering small islands, can become complicated.

Apparently FE methods have never been used for wave propagation models. FE methods may be useful for wave models as they present a natural way to increase model resolution in places where such resolution is needed (typically along coast lines). However, it remains to be seen if matrix solvers implicit to FE methods can be made efficient for the large number of degrees of freedom required in a wave model. Because this study is intended to use existing techniques, FE methods will not be considered further.

FD methods have often been used in wave models. A distinction is made between explicit and implicit schemes. To the knowledge of the author, only explicit schemes have been used in wave models. Explicit schemes have the advantage of being relatively simple to implement, and have relatively modest computer memory requirements. Their disadvantage is that time steps are limited by Courant-Friedrich-Lewy (CFL) criteria. For high resolution models, this usually implies that the propagation time step becomes much smaller than the time step of the physical processes involved. Implicit FD methods are generally designed to be unconditionally stable, and therefore do not have the above time step limitation. However, implicit methods usually require more memory, which, given the large number of degrees of freedom in wave models, can be a problem. Furthermore, implicit FD methods in

4

general are more difficult to implement than explicit methods.

Considering the above, three types of propagation schemes are potentially suitable for implementation in third-generation wave models; partial ray (semi-Lagrangian) methods, and explicit or implicit FD schemes. The present study will concentrate on the simplest of these three methods; the explicit FD methods. The need/potential for other methods will be discussed at the end of this report.

3 Selection and testing of a propagation scheme

Many explicit FD methods have been used in wave models (see, for instance, SWAMP group 1985; Neu and Won 1990; Tolman 1991, 1992). Furthermore, Eq. (5) is similar to the governing equation in transport and pollution models. In this field, a wealth of experience exists (see, for instance, Fletcher 1988; Cahyono 1994), which can be applied directly to wave models.

Before a numerical scheme can be selected, requirements have to be formulated. Based on several years of experience with developing and operating third-generation wave models, the following four requirements are considered:

1 The scheme has to result in accurate propagation of poorly resolved swell fields over large distances at an angle with the spatial grid.

2 The scheme has to be able to deal with extremely poor resolutions, in particular, with respect to spectral directions (see Booij and Holthuijsen 1987).

3 The scheme should result in negligible spurious oscillations and/or negative wave energy.

4 When combined with source terms, the scheme should result in stable fetch-limited growth.

The first two requirements are straightforward, although not easy to quantify. The latter two requirements address the occurrence of dispersion errors in higher order schemes. Such errors manifest as wave-like spurious solutions trailing or leading a propagated wave field of finite dimensions (see, for instance, Fletcher 1988). Such spurious solutions result in negative wave energy, and may interact with the source terms (in particular the sensi-

5

tive nonlinear interactions), resulting in temporal oscillation of solutions for steady conditions. For many schemes such oscillations are small and damp out slowly, but for some schemes, they result in unstable model behavior. This interaction with source terms may require additional numerical diffusion or filtering to stabilize results (e.g., Tolman 1991, 1992). This will be discussed in section 6.

The first requirement implies the need for a higher-order accurate scheme, as will be illustrated below. All explicit higher order schemes, however, result to some degree in the above discussed spurious oscillations for poorly resolved fields. Three groups of solution techniques are available to minimize this problem (see, for instance, Fletcher 1988). These are Flux Corrected Transport (FCT) schemes, Total Variance Diminishing (TVD) schemes and filters and Total Variance Bounded (TVB) schemes and filters. Furthermore, many 'engineering' solutions are available (see, for instance, Tolman 1991).

Although some experience has been obtained with higher-order propagation schemes in wave models, this experience is generally limited. There is, however, an abundance of experience with the numerical solution of similar type equations in the field of pollution and transport models. Instead of starting a separate comparative study into the behavior of numerical schemes for wave models, the latter experience should be used. One of the most recent comprehensive studies in this field has been performed by Cahyono (1993) and Falconer and Cahyono (1993). This study indicates that the best balance between accuracy and economy is obtained by using the QUICKEST scheme (Leonard 1979), in combination with the ULTIMATE TVD limiter (Leonard 1991). This scheme is third-order accurate in both space and time. It does, however, require splitting of the solution in all separate dimensions, effectively making the scheme second-order accurate in space and time. Below, the ULTIMATE QUICKEST scheme will be denoted as the UQ scheme.

We will consider the UQ scheme for propagation in one dimension first. The QUICKEST scheme is based on the fluxes between cell boundaries. The discrete flux $\mathcal{F}_{i,-}$ between grid points with indices i and $i-1$ is defined as

$$\mathcal{F}_{i,-} = \frac{\Delta t}{\Delta x} \left(\dot{x}_b \, F_b \right) , \qquad (6)$$

where $\dot{x} = c_g$ [Eq. (2)], and where the suffix b indicates values at the cell boundary, defined as

6

$$\dot{x}_b = 0.5\left(\dot{x}_i + \dot{x}_{i-1}\right) , \tag{7}$$

$$F_b = \frac{1}{2}\left[(1+C)F_{i-1} + (1-C)F_i\right] - \left(\frac{1-C^2}{6}\right)\mathcal{CU}\,(\Delta x)^2, \tag{8}$$

where C is the CFL number at the cell boundary (including a sign identifying the propagation direction)

$$C = \frac{\dot{x}_b\,\Delta t}{\Delta x} , \tag{9}$$

and $\mathcal{CU}$ is the (upstream) curvature of the energy density distribution

$$\mathcal{CU} = \begin{cases} \left(F_{i-2} - 2F_{i-1} + F_i\right)(\Delta x)^{-2} & \text{for} \quad C \geq 0 \\ \left(F_{i-1} - 2F_i + F_{i+1}\right)(\Delta x)^{-2} & \text{for} \quad C < 0 \end{cases} . \tag{10}$$

To assure that this scheme does not generate aphysical extremata, it is used in combination with the ULTIMATE limiter. This limiter uses the central, upstream and downstream energy density (suffices c, u and d, respectively), which are defined as

$$\begin{array}{llll} F_c = F_{i-1} , & F_u = F_i , & F_d = F_{i-2} & \text{for} \quad C \geq 0 \\ F_c = F_i , & F_u = F_{i-1} , & F_d = F_{i+1} & \text{for} \quad C < 0 \end{array} , \tag{11}$$

To assess if the initial state and the solution show similar monotonic or non-monotonic behavior, the normalized energy $\tilde{F}$ is defined as

$$\tilde{F} = \frac{F - F_u}{F_d - F_u} . \tag{12}$$

If the initial state is monotonic (i.e., $0 \leq \tilde{F}_c \leq 1$), the (normalized) energy at the cell boundary F_b is limited to

$$\tilde{F}_c \leq \tilde{F}_b \leq 1 \ , \quad \tilde{F}_b \leq \tilde{F}_c\,C^{-1} \ . \tag{13}$$

otherwise

$$\tilde{F}_b = \tilde{F}_c . \tag{14}$$

This completes the calculation (and limitations) of the fluxes at the cell boundaries. The actual propagation scheme then follows from applying these fluxes to the spectral density at the grid point.

$$F_i^{n+1} = F_i^n + \mathcal{F}_{i,-} - \mathcal{F}_{i,+} \,, \tag{15}$$

where $\mathcal{F}_{i,+} = \mathcal{F}_{i+1,-}$ and n is the discrete time index.

This completes the description of the UQ scheme except for the treatment of boundary conditions. Boundary treatment is required if one of the grid points is either on land (where $F = 0$ is assumed) of is a point with a predefined boundary value. In such cases, Eqs. (7) and (8) are replaced by

$$\dot{x}_b = \dot{x}_s \,, \tag{16}$$

$$F_b = F_u \,, \tag{17}$$

where the suffix s indicates the (average of) the sea point(s). This boundary condition represents a simple first order upwind scheme, which does not require the limiter (11) through (14).

Stability requirements for the UQ scheme are similar to those of a first order scheme, where the Courant number $|C|$ has to be less than 1.

Before applying this scheme to multi-dimensional tests, some simple one-dimensional test cases are considered. First consider a test similar to that of Tolman (1992), Fig. 6. The initial distribution of the significant wave height is given by

$$H_s = \int_0^{2\pi} \int_0^\infty F(f,\theta)\, df\, d\theta \,, \tag{18}$$

is Gaussian in space. All energy is concentrated in a single spectral bin, representing monochromatic swell. This wave height distribution is propagated for 100 time steps with $C = 0.28$. Results for a conventional first order scheme and the UQ scheme are shown in Fig. 1a. The advantages of the latter scheme over the first order scheme are obvious. This scheme nevertheless results in an error in the maximum value of F of approximately 10%, and tends to flatten the maximum and sharpen the transition to areas without wave

8

energy. Both are known properties of TVD and FCT schemes. It might appear that the present scheme performs poorer than the SHASTA scheme as used by Tolman (1991). Extended experience with the SHASTA scheme, however, has shown that this scheme tends to skew energy distributions, in particular for large CFL numbers, and does not interact well with source terms (see section 6). On first impression, Fig. 1a suggests that the first order scheme generates wave energy, because the surface under the distribution predicted by the first order scheme is much larger than that of the exact solution. This, however, is not the case. The wave energy, which corresponds to H_s^2, is conserved by both schemes.

The above one-dimensional test is fairly typical for tests of advection schemes, but not necessarily relevant for swell propagation over long distances. As an extreme swell propagation test, propagation of long swell around the globe will be considered. Swell is considered with a period $T = 24.9s$, which travels around the world in 24 days. The grid increment is chosen as $\Delta x = 1°$, and the time step as $\Delta t = 1h$ (576 time steps). The initial conditions again consist of a Gaussian wave height distribution in space with a standard deviation of Δx, $2\Delta x$ or $4\Delta x$. The results for a conventional first order scheme and the UQ scheme are shown in Fig. 1b through d, respectively. For all three cases the superior behavior of the UQ scheme compared to the first order scheme is again obvious, and errors of the UQ scheme are similar to those in Fig. 1a. The case shown in Fig. 1b represents a wave field which is poorly resolved by the grid. In this case, no numerical scheme can be expected to propagate the swell field accurately. The error in the maximum swell height for the UQ scheme is approximately 44%, which is still a major improvement over the error in the first order scheme (76% underestimation of the peak wave height). The case shown in Fig. 1c represents a wave field which is reasonably well resolved. In this case the error of the higher order scheme is reduced to 22%, compared to 66% for the first order scheme. Finally, Fig. 1d represents a well resolved case, where the errors of both schemes are 6% and 53%, respectively. For the latter two cases the behavior of the UQ scheme is excellent, particularly considering the severity of the test.

For propagation in multiple dimensions, propagation in each dimension is considered using a separate fractional step. Accuracy, in particular near boundaries can be improved by rotating the order of the fractional steps. A

9

two-dimensional implementation of the QUICKEST scheme has been suggested by Davis and More (1982). This scheme, however, is only first order accurate in time due to the omission of some cross-derivatives (see, e.g., Fletcher 1988, p. 344). For propagation of wave energy at an angle with the grid this leads to an unacceptable deformation of the propagated energy distribution (figures not presented here). Note that Cahyono (1993) also concluded that the implementation of the UQ scheme using a splitting technique for all dimensions is more accurate than the Davis and More version of this scheme.

Several two-dimensional propagation tests have been performed. The first test considers straightforward propagation of swell in deep water under several angles with the grid. Swell again is described by considering wave energy in a single discrete spectral bin. The two-dimensional spectral propagation equation for this case is given as

$$\frac{\partial F}{\partial t} + \frac{\partial}{\partial x}\dot{x}F + \frac{\partial}{\partial y}\dot{y}F = 0 \,, \tag{19}$$

where x and y represent the two spatial dimensions, $\dot{x} = c_g \cos\theta$, and $\dot{y} = c_g \sin\theta$. Test results for the two schemes considered here are presented in Fig. 2. The initial condition (panel a) consists of a swell field with a Gaussian wave height distribution with a spread of $2\Delta x$ and $2\Delta y$ in the two spatial dimensions, where spatial increments are identical ($\Delta x = \Delta y$). Thus, this test represents a reasonably well resolved wave field. The exact solution consists of a propagation of the field over a distance $37.5\Delta x = 37.5\Delta y$ in the wave propagation direction θ, without a change in the shape of the spatial distribution. Fig. 2b and c show the results for the first order scheme for (Cartesian) directions $\theta = 0°$ and $45°$, respectively. As expected, these results show large numerical diffusion, with errors in the maximum wave height of 32% and 48%, respectively. Moreover, the orientation of the numerical diffusion is sensitive to the propagation direction θ, which is obviously not desirable. Finally, the propagation velocity, in particular across the grid, appears slightly slow. Figs. 2d and e show the corresponding results for the UQ scheme. Although the errors of this scheme are not negligible (8% and 16%, respectively), they are much smaller than for the first order scheme. This scheme tends to transform the original distribution to a somewhat more square shape, but keeps the energy close to the target area. Although the change in shape of the wave height distribution is somewhat dependent on

the propagation direction, this is much less obvious than with the first order scheme. The UQ also appears to be somewhat slow in propagating the wave fields, but less so than the first order scheme.

The second two-dimensional propagation test considers swell propagation across the Pacific Ocean using realistic model resolutions. Most global or large scale wave models are defined in terms of longitude λ and latitude ϕ. The corresponding balance equation for deep water becomes (e.g., Groves and Melcer 1961;WAMDIG 1988)

$$\frac{\partial F}{\partial t} + \frac{1}{\cos\phi}\frac{\partial}{\partial\phi}\dot{\phi}\,\cos\phi\,F + \frac{\partial}{\partial\lambda}\dot{\lambda}F + \frac{\partial}{\partial\theta}\dot{\theta}_g F = 0 \,, \qquad (20)$$

$$\dot{\phi} = \dot{y}\,R^{-1} \,, \qquad (21)$$

$$\dot{\lambda} = \dot{x}\,(R\,\cos\phi)^{-1} \,, \qquad (22)$$

$$\dot{\theta}_g = \dot{x}\,\tan\phi\,R^{-1} \,, \qquad (23)$$

where R is the radius of the earth, and $\dot{\theta}_g$ represents the change in direction of waves propagating along great circles. Note that this equation is easily transformed to shallow water by using the corresponding expressions for $\dot{x}$ and $\dot{y}$, and by combining the refraction velocities (3) and (23). Note furthermore that Eq. (20) can be rewritten as

$$\frac{\partial\mathcal{A}}{\partial t} + \frac{\partial}{\partial\phi}\dot{\phi}\mathcal{A} + \frac{\partial}{\partial\lambda}\dot{\lambda}\mathcal{A} + \frac{\partial}{\partial\theta}\dot{\theta}_g\mathcal{A} = 0 \,, \qquad (24)$$

where the propagated quantity $\mathcal{A} \equiv F\cos\phi$. Consequently, the above propagation schemes can be used without modification on the propagated quantity $\mathcal{A}$. A deep-water swell propagation model has been constructed for the Pacific Ocean based on Eq. (24), using a spatial resolution $\Delta\phi = 1°$ and $\Delta\lambda = 1.25°$, and a time step of 20 min. Even for longcrested swell, a discrete description of the spectral direction is required, due to the great-circle refraction term in Eq. (24). Following common practice in wave modeling, we have chosen $\Delta\theta = 15°$. The initial condition consists of a swell field with a period $T = 17$s, south of Kamchatka. Its center is located at 160°E and 45°N, and the swell field has a Gaussian wave height distribution in space with a spread of $2\Delta\lambda$ and $2\Delta\phi$ (2.5° and 2.0°, respectively). To represent swell that has been generated recently, the directional distribution of wave energy in the

11

spectrum $F(f, \theta)$ is of the form $\cos^2(\theta - \bar{\theta})$, where $\bar{\theta}$ is the mean propagation direction. Such a directional distribution is fairly representative for wind seas. Two cases are considered; in the first case swell is propagating mainly to the east with $\bar{\theta} = 120°$ relative to North (oceanographic convention), and in the second case mainly to the south with $\bar{\theta} = 150°$.

Before assessing the behavior of the two schemes considered here, the exact solution will be approximated. This approximation is obtained by considering the results of the UQ scheme for good resolutions in all spaces considered. For this purpose a model with $\Delta\lambda = \Delta\phi = 0.25°$ and $\Delta\theta = 2.5°$ has been constructed. The corresponding spatial resolution is more than a factor of 2 better than the best resolution in Fig. 2. The directional resolution is sufficient to avoid effects of discrete dispersion as described by Booij and Holthuijsen (1987). It is expected that the error of the wave heights thus obtained is of the order of 10% or smaller. The initial conditions, and the 'exact' solutions after 2, 4 and 6 days are shown in Figs. 3 and 4, and the evolution of the maximum wave height is presented in Fig. 5. The swell field propagates with identical speed in all directions contained in the initial wave field. The large initial directional spread results in a crescent-shaped wave height distribution which covers an increasing area with increasing time. Due to this directional dispersion, the maximum wave height decreases to 38%, 28% and 24% of the initial maximum wave height after 2, 4 and 6 days, respectively (see Fig. 5). Apart from effects of coastlines and the distortions due to the map projection, the wave fields for both cases are very similar, as expected. Note that in nature dispersion also occurs in the propagation direction of the swell, as even swell shows a distribution of wave energy over a continuum of frequencies. Because this test case considers purely monochromatic swell, frequency dispersion does not occur. The effect of frequency dispersion will be discussed in section 4.

The expected reduction of the maximum swell height due to directional dispersion can be estimated by considering the asymptotic behavior of swell propagating from a point source. In this case the swell fields at different times are located on concentric circles. The area over which the wave energy in any part of the directional distribution is spread due to directional dispersion is then proportional to the circumference C of the circle on which the swell field resides, where c is given as

$$C = R \, \sin\left(\frac{c_g t}{R}\right) . \tag{25}$$

Conservation of energy requires the swell energy to be inversely proportional to C, so that the wave height H_S becomes proportional to

$$H_s \propto \left[R \, \sin\left(\frac{c_g t}{R}\right)\right]^{-1/2} . \tag{26}$$

For propagation distances $c_g t$ significantly smaller than R these two equations can be approximated as

$$C = c_g t , \tag{27}$$

$$H_s \propto t^{-1/2} . \tag{28}$$

The above asymptotic solutions are valid only if the propagation distance $c_g t$ is significantly larger than the spatial extent of the initial distribution. In the tests considered, this is the case after approximately 1 day (note that Eq. 26 requires that $H \uparrow \infty$ for $t \downarrow 0$). The trend of Eq. 26 is included in Fig. 5. After approximately one day, the wave height reduction due to directional dispersion (solid lines) follows the behavior of Eq. 26 (dotted line) perfectly.

Figures 6 and 7 show the results for the first order scheme using the above realistic model resolutions, and Figs. 8 and 9 show the corresponding results for the UQ scheme. Both schemes show peculiar results with several local maxima.

The only difference between 'exact' model of Figs. 3 and 4 and the UQ scheme of Figs. 8 and 9 is the numerical resolution. The reduced spatial resolution results in a slight deformation of the propagated wave field. The narrow distribution of wave heights in the propagation direction of the waves is nevertheless maintained. The effect of the reduced directional resolution is much more dramatic. In Figs. 8 and 9 the initial condition consists of a set of discrete wave fields for directional increments of 15°. All these wave fields propagate more or less independently, resulting in a set of local maxima along the crescent shaped wave field. This is the so-called garden sprinkler effect (Booij and Holthuijsen 1987, henceforth denoted as GSE), which occurs for any accurate scheme if the directional resolution is insufficient to maintain

the continuity of the wave field. The required directional resolution to avoid the GSE is of the order of $\Delta\theta = \Delta x/(c_g t)$, which is typically of the order of 1° to 3°.

In the first order scheme (Figs. 6 and 7), the GSE is not obvious. It is masked by the large numerical diffusion of this scheme, which is particularly evident in the large spreading of the wave field in the wave propagation direction. This scheme only appears to favor propagation along meridians, generating an additional local maximum at 160°. The generation of this local maximum is caused by the formulation of the balance equation (20) in terms of longitudes (λ) and latitudes (ϕ). Waves propagating along meridians remain on the same meridian, because it is a great circle. Then $\dot{\lambda} = \dot{\theta}_g = 0$, and the propagation is essentially one-dimensional. Numerical diffusion then occurs only along the propagation direction (compare Fig. 2b and Fig. 10). Because wave energy is not redistributed perpendicular to the wave propagation direction, the GSE remains noticeable. For all other propagation directions great circles are curved lines in ϕ-λ space, so that the propagation is three-dimensional. This implies that the first order scheme introduces significant numerical diffusion in the ϕ, λ and θ spaces. The numerical diffusion in λ and ϕ space simply manifests itself as a spreading of wave energy in these spaces. The numerical diffusion in θ space, manifests itself as a spreading of wave energy perpendicular to the wave propagation direction (see Fig. 10). Consequently, waves not travelling along meridians are subject to large numerical diffusion in all directions. This diffusion is apparently sufficient to mask the GSE for the model resolutions considered here.

Two additional remarks need to be made considering the GSE. First, the directional dispersion of swell results in a continuous narrowing of the directional distribution. The directional distribution of swell energy is therefore always poorly resolved by practical model resolutions. *Every* propagation scheme will therefore result in some numerical diffusion in θ space due to the great circle refraction term. This effect will be largest for components travelling at large angles with meridians, for which the great-circle refraction velocity is largest. In Figs. 8 and 9 this effect can be observed as a slightly smoother wave height distribution for waves traveling in the most easterly directions. Secondly, the (relative) effect of the curvature of great circles in λ-ϕ space becomes smaller for small-scale models and near the equator. In such conditions propagation along parallels will become nearly one-dimensional, and the first order scheme can be expected to favor this propagation direction

14

too.

Figure 5 shows the evolution of the maximum wave height in time for the first order scheme (chain lines). For the first three days, the maxima of both runs with the first order scheme are practically identical, as would be expected. In the last three days, the results of both runs start to deviate. This is attributed to the occurrence of the spurious maximum at 160°E. When this maximum becomes the global maximum, the reduction of the maximum wave height slows down significantly (branch marked A in figure). The maximum wave height predicted by the first order scheme is systematically low (compare chain and dotted lines), as would be expected considering the large numerical diffusion of this scheme. Figure 5b furthermore shows that the rate of reduction of the maximum wave height is too large (compare the slopes of the chain and dotted lines), except when the spurious maximum becomes the maximum wave height (branch marked A).

The evolution of the maximum wave height of the UQ scheme is also presented in Fig. 5 (dashed lines). The results for both runs are again similar, until a spurious maximum at 160°E becomes the global maximum in the run with southerly wave propagation (branch marked B in the figure). In the latter case the wave height reduction due to dispersion stops almost completely. The maximum wave height predicted by the UQ scheme follows the exact solution closely, in spite of the unrealistic spatial energy distribution. This behavior is attributed to cancellation of numerical errors; the local maxima in the swell distribution are expected to over-estimate the maximum wave height, whereas propagation errors of these local maxima reduce the predicted wave height.

The clear occurrence of the garden-sprinkler effect and unrealistic dispersion characteristics of accurate schemes like the UQ scheme, show that the improvement of the numerical scheme in some ways degrades model performance. The solution to this problem is simple: increase the directional resolution by an order of magnitude. This solution, however, is usually not economically feasible. An alternative solution is discussed in the following section.

4 Dispersion correction

The GSE and solutions to this problem have been discussed in detail by Booij and Holthuijsen (1987). Their solution adds a diffusion tensor to the propagation equation. Considering plane-grid propagation without a refraction term, their equation becomes

$$\frac{\partial F}{\partial t} + \frac{\partial}{\partial x}\left[\dot{x}F - D_{xx}\frac{\partial F}{\partial x}\right] + \frac{\partial}{\partial y}\left[\dot{y}F - D_{yy}\frac{\partial F}{\partial y}\right] - 2D_{xy}\frac{\partial^2 F}{\partial x \partial y} = 0 , \quad (29)$$

$$D_{xx} = D_{ss} \cos^2\theta + D_{nn} \sin^2\theta , \quad (30)$$

$$D_{yy} = D_{ss} \sin^2\theta + D_{nn} \cos^2\theta , \quad (31)$$

$$D_{xy} = (D_{ss} - D_{nn}) \cos\theta \sin\theta , \quad (32)$$

$$D_{ss} = (\Delta c_g)^2 T_s/12 , \quad (33)$$

$$D_{nn} = (c_g\Delta\theta)^2 T_s/12 , \quad (34)$$

where D_{ss} is the diffusion coefficient in the propagation direction of the wave component, D_{nn} is the diffusion coefficient perpendicular to the wave propagation direction, Δc_g is the discrete increment of group velocities corresponding to the discrete frequency increment Δf, and T_s is the time elapsed since the generation of the swell (henceforth denoted as the 'swell age'). The diffusion along the main axes of the tensor D_{ss} and D_{nn} depends on the spectral increments Δf and $\Delta\theta$. Hence the required numerical diffusion decreases with increasing resolution. For third generation wave models, a logarithmic frequency grid is used, where $\Delta f = X_f f$, and X_f is typically 0.1. For deep water, this implies that $\Delta c_g = X_f c_g$. The ratio between D_{ss} and D_{nn} then becomes

$$\frac{D_{ss}}{D_{nn}} = \left(\frac{X_f}{\Delta\theta}\right)^2 , \quad (35)$$

which for $X_f = 0.1$ and $\Delta\theta = 15°$ becomes 0.15. Hence the diffusion perpendicular to the wave propagation direction D_{nn} is an order of magnitude larger than the diffusion in the propagation direction D_{ss}. This implies that

16

the diffusion will mainly redistribute wave energy perpendicular to the propagation direction (i.e., along the crescent shaped swell fields), whereas the widening of the the swell field in the propagation direction will be less.

Equation (29) cannot be used directly in combination with the UQ scheme, because this scheme treats two-dimensional propagation as essentially one-dimensional. Therefore, a separate diffusion step is added to the propagation algorithm.

$$\frac{\partial F}{\partial t} = \frac{\partial}{\partial x}\left[D_{xx}\frac{\partial F}{\partial x}\right] + \frac{\partial}{\partial y}\left[D_{yy}\frac{\partial F}{\partial y}\right] + 2D_{xy}\frac{\partial^2 F}{\partial x \partial y} \, . \tag{36}$$

Note that this also allows for a simple reintroduction of refraction, and for transferring the equation to a longitude-latitude grid (i.e., again replacing F by $\mathcal{A}$). This equation is solved using a simple forward-time central-space scheme. At the cell interface between points i and $i-1$ in x space, the term in brackets in the first term on the right side of Eq. (36) (denoted as $\mathcal{D}_{i,-}$) is estimated as

$$D_{xx}\frac{\partial F}{\partial x} \approx \mathcal{D}_{i,-} = \left(\frac{D_{xx,i}+D_{xx,i-1}}{2}\right)\left(\frac{F_i - F_{i-1}}{\Delta x}\right) \, . \tag{37}$$

Corresponding values for indices i and $i+1$ ($\mathcal{D}_{i,+}$), and for gradients in y space ($\mathcal{D}_{j,-}$ and $\mathcal{D}_{j,+}$) are obtained by rotating indices. If one of the two grid points is located on land, the discrete diffusion between the grid points is set to zero. The mixed derivative at the right side of Eq. (36) is estimated for the grid point indices i and $i-1$ in x-space and j and $j-1$ in y-space as

$$D_{xy}\frac{\partial^2 F}{\partial x \partial y} \approx \mathcal{D}_{ij,--} = \left(\frac{D_{xy,i,j}+D_{xy,i-1,j}+D_{xy,i,j-1}+D_{xy,i-1,j-1}}{4}\right)$$
$$\times \left(\frac{-F_{i,j}+F_{i-1,j}+F_{i,j-1}-F_{i-1,j-1}}{0.5(\Delta x_j + \Delta x_{j-1})\,\Delta y}\right) \quad . \tag{38}$$

Note that the increment Δx will become a function of y if a longitude-latitude grid is used. This term is evaluated only if all four grid points considered are sea points, otherwise it is set to zero. Using a forward-in-time discretization of the first term in Eq. (36), and space-centered discretizations

for the remainder of the first and second term on the right side, the final numerical representation of Eq. (36) becomes

$$F_{i,j}^{n+1} = F_{i,j}^n + \frac{\Delta t}{\Delta x} \left(\mathcal{D}_{i,+} - \mathcal{D}_{i,-} \right) + \frac{\Delta t}{\Delta y} \left(\mathcal{D}_{j,+} - \mathcal{D}_{j,-} \right)$$
$$+ \frac{\Delta t}{4} \left(\mathcal{D}_{ij,--} + \mathcal{D}_{ij,-+} + \mathcal{D}_{ij,+-} + \mathcal{D}_{ij,++} \right) . \qquad (39)$$

Using this forward-in-time and central-in-space scheme, stable solutions can be obtained for (e.g., Fletcher 1988, Part I section 7.1.1)

$$\frac{D_{\max} \Delta t_g}{\min(\Delta x, \Delta y)^2} \leq 0.5 , \qquad (40)$$

where $D_{\max}$ is the maximum value of the diffusion coefficient (typically $D_{\max} = D_{nn}$). This implies that for old long swells, where both c_g and T_s in Eq. (34) are large, stability can become a serious problem, particularly for high-resolution grids (small Δx and Δy).

In testing this diffusive dispersion correction and comparing it to the 'exact' solution of Fig. 3, one should realize that the exact solution considers only monochromatic waves (a single frequency), instead of the more natural continuous frequency spectrum. The exact solution therefore does not include frequency dispersion as described above by D_{ss}. For the swell propagation tests with the diffusive dispersion correction we therefore compare the exact solution to numerical results with $D_{ss} \equiv 0$. Below we will denote the UQ scheme with the diffusive dispersion correction as the UQDC scheme.

Figures 11 and 12 shows results for the UQDC scheme with $D_{ss} \equiv 0$. The swell age T_s is set to 0 for the initial condition, and evolves naturally during propagation ($dT_s/dt = 1$). The resulting wave fields remain realistically narrow in the wave propagation direction, but are much smoother perpendicular to the wave propagation direction than the results of the UQ scheme (Figs. 8 and 9). Some local maxima can still be distinguished, but the local maximum at 160°E no longer becomes the global maximum. The evolution of the maximum wave height is shown in Fig. 13 (chain lines). The predicted maximum wave height is somewhat smaller than the exact solution, but fol-

18

lows the dispersion trend closely. The maximum wave height for both runs remain nearly identical, as the local maximum at 160°E no longer dominates.

The dynamic evolution of the swell age T_s introduces two practical problems. The first is the above recognized stability problem, which cannot be evaluated easily if T_s is allowed to evolve dynamically. The second problem is the definition of T_s for realistic wave conditions considering multiple swell fields and a wind sea. T_s could be evaluated using a balance equation similar to that of the spectrum F (Booij and Holthuijsen 1987, appendix). This roughly doubles the memory required for a wave model, which is generally not acceptable in an operational environment. However, Booij and Holthuijsen also suggest (p. 322) that the use of a single representative wave age T_s might be adequate for the description of swell propagation. A singe wave age simplifies the assessment of numerical stability, and requires a negligible increase in memory for implementation of the diffusive correction.

Figures 14 and 15 show results for the UQDC scheme with $D_{ss} \equiv 0$ and $T_s = 5$ days. Like in the test with the dynamically evaluated swell age T_s, a good representation of the exact solution is found. Due to the fairly large diffusion selected, the secondary maxima have been suppressed even further compared to Figs. 11 and 12. The stronger diffusion results in an additional (small) underestimation of the maximum wave height (dashed lines in Fig. 13), but does not influence the dispersion behavior (slope of dashed lines in Fig. 13).

Note that with the simplified description of D_{ss} and D_{nn}, it is also reasonable to assume that the diffusion coefficients are constant over the grid, and to use the deep water diffusion coefficients everywhere. Equations (37) and (38) can then be simplified as

$$\mathcal{D}_{i,-} = D_{xx} \left(\frac{F_i - F_{i-1}}{\Delta x} \right) . \tag{41}$$

$$\mathcal{D}_{ij,--} = D_{xy} \left(\frac{-F_{i,j} + F_{i-1,j} + F_{i,j-1} - F_{i-1,j-1}}{0.5(\Delta x_j + \Delta x_{j-1})\,\Delta y} \right) , \tag{42}$$

which for deep water and a single swell source (or a constant T_s) are identical to Eqs. (37) and (38).

5 Frequency dispersion

Swell with a single frequency has been considered up to this point, ignoring effects of dispersion due to the continuous frequency spectrum of every wave field. For pure frequency dispersion (ignoring directional dispersion) the asymptotic solution for waves originating from a point source shows a decay of the (maximum) wave proportional to the inverse root of the time t (e.g., Whitham 1974, chapters 11 and 13)

$$H_s \propto t^{-1/2} . \tag{43}$$

Multiplication with Eqs. (26) or (28) to obtain the dispersion rate for both directional and frequency dispersion then results in

$$H_s \propto \left[tR \ \sin \left(\frac{c_g t}{R} \right) \right]^{-1/2} , \tag{44}$$

$$H_s \propto t^{-1} , \tag{45}$$

as a general solution, and a solution for short distances, respectively.

Due to economical constraints, it is virtually impossible to generate an 'exact' solution for full spectral propagation by using high resolution in all spaces considered. Therefore, model results for realistic model resolutions will only be compared to each other and to the dispersion trend predicted by Eq. (44). Considered is the propagation of a JONSWAP spectrum (Hasselmann et al. 1973) with a peak period of 17 s, a peak-enhancement factor $\gamma = 3.3$, and the directional distribution of Hasselmann et al. (1980). The frequency resolution is given as $f_{i+1} = 1.1f_i$. The corresponding one-dimensional input spectrum is presented in Fig. 16a. Only the eastern propagation direction with $\bar{\theta} = 120°$ is considered. The results for the first order scheme, the UQ scheme, the UQDC scheme with dynamically evaluated T_s, and the UQDC scheme with constant T_s are presented in Figs. 17 through 20, respectively

The first order scheme (Fig. 17), shows the expected smooth behavior, with a minor spurious maximum at 160°E. Because this solution is significantly influenced by numerical diffusion, it is attractive, as it produces fairly physical wave height distributions. In contrast, the UQ scheme (Fig. 18), shows disintegration of the wave field. Such results are clearly unacceptable for practical wave models. The two versions of the UQ scheme with the

20

diffusive dispersion correction (Figs. 19 and 20) successfully remove the disintegration from the UQ scheme, and show results which are similarly smooth as those of the first order scheme. The maximum wave heights, however, occur in a more defined region (without a spurious maximum at 160°W), and the corresponding spectra are much sharper (figures not presented here).

The evolution of the maximum wave height predicted by the above four schemes is presented in Fig. 21. As expected, the wave height decay is more rapid than in the previous monochromatic, short-crested cases (compare with Fig. 5). Furthermore, the first order scheme results in the smallest wave heights. The differences between the schemes, however, have become smaller. This is due to the fact that the higher order scheme now incorporates additional diffusion (D_{ss}), whereas the first order scheme remains unchanged compared to the monochromatic cases. Unfortunately, none of the schemes reproduces the trend of Eq. (44) particularly well. In fact, the decay rate of the first order scheme appears to be the most realistic.

The poor description of frequency dispersion for the conventional spectral resolution is likely related to poor resolution of the frequency spectrum. Figure 16a shows that most of the input energy is concentrated in a single spectral bin. This implies that effects of reduction of the wave height due to the different propagation velocities of spectral components will not be modelled accurately. In fact, most of the frequency dispersion in the model is generated by the diffusion term in the dispersion correction equation. To test this hypothesis, calculations have been performed with a higher frequency resolution $(f_{i+1} = \sqrt{1.1}f_i)$, and with a smoother spectrum (peak enhancement factor $\gamma = 1$, i.e., a Pierson-Moskowitz spectrum). The corresponding initial spectrum is shown in Fig. 16b. Note that the peak of this spectrum is relatively well resolved by the frequency discretization.

The results for the first-order scheme and the UQDC scheme with $T_s = 5$ days using the enhanced spectral resolution are presented in Figs. 22 and 23, respectively. Due to the smoother spectrum, wave energy is spread over a larger area in the propagation direction of the waves, and apart from the spurious maximum at 160°E in the first order scheme, the results of both schemes are similar. The evolution of the maximum wave heights for both schemes is presented in Fig. 24. The maximum wave heights for both schemes indeed appear very similar, and follow the expected dispersion behavior (dotted lines) closely. The latter confirms that the poor representation of frequency dispersion in conventional model resolutions and a strongly peaked spectrum

are caused by insufficient resolution in the frequency space.

The close similarity between the results of the the first-order scheme and the UQDC scheme with respect to the maximum wave height and the wave height distribution do not necessarily imply that the details of the wave fields are also similar. To assess some details of the wave field, time series of some additional parameters will be considered for the location 160°W and 20°N. First, Fig. 25 shows local wave heights for the calculations with the conventional frequency resolution (panel a) and for the enhanced resolution (panel b). The UQDC scheme (solid lines) results in maximum wave heights 10 to 20% higher than those of the first order scheme (dotted lines), and the maximum wave heights occur over a shorter time interval. The corresponding spectra, however, show much larger differences. This can be illustrated by considering the peak frequency f_p presented in Fig. 26. For a point source, the expected peak frequency at a distance r from a source in deep water is

$$ f_p = \frac{gt}{4\pi r} , \qquad (46) $$

where t it the time elapsed since wave generation (Snodgrass et al. 1966). This analytical solution is shown as the dashed line in Fig. 26. For the conventional spectral resolution and the JONSWAP spectrum (Fig. 26a), the first order scheme (dotted line) represents the change of peak frequency poorly. During the passage of the maximum swell height, the peak frequency remains nearly unchanged for more than a day. The UQDC scheme shows a significantly better reproduction of the expected evolution of f_p, but also includes noticeable errors. For the enhanced frequency distribution and the Pierson-Moskowitz spectrum (panel b), the first order scheme (dotted line) shows much better results, but significantly overestimates the peak frequency before the maximum wave height occurs, and underestimates it afterward. The UQDC scheme shows much smaller errors.

Errors in the peak frequency and hence in the local spectra imply that the spatial and temporal evolution of the wave field are not well described. This becomes obvious, if the source area of the swell field is reconstructed from the evolution of the peak frequency at 160°W 20°N. Differentiating (46) with respect to time, results in

$$r = \frac{g}{4\pi} \left(\frac{\partial f_p}{\partial t} \right)^{-1} . \tag{47}$$

Such estimates of r are presented in Fig. 27 for the models with the conventional resolution (panel a) and with the enhanced resolution (panel b). The results show some noise related to round-off errors in f_p that occur in Eq. (47), but most of the oscillations are due to frequency discretization in combination with numerical propagation errors. For the conventional frequency resolution (panel a), the first order scheme (dotted line) overestimates the distance of the swell source by an order of magnitude during the passage of the maximum swell height. The errors of the UQDC scheme (solid line) are clearly smaller, but still unacceptably large. For the high-resolution model, the first order scheme shows a systematic overestimation of the source distance r of 50-100%. The UQDC scheme is clearly more accurate, but also shows a systematic overestimation of the distance before the swell peak has passed ($t < 4$ days). The differences between panels a and b again suggest that most of the errors in panel a are related to the insufficient frequency resolution.

6 Fetch-limited wave growth

The final test of the propagation scheme considered here is its interaction with source terms. Previous experience with higher order accurate propagation schemes shows that such schemes might produce spurious oscillations in steady fetch-limited growth curves and even influence model instability (Tolman 1991, 1992). This behavior is probably related to the interaction between nonlinear source terms and numerical dispersion errors in the propagation scheme. To investigate the interaction between propagation schemes and source terms we consider a simple case of one-dimensional fetch-limited wave growth in deep water. The corresponding spectral energy balance equation is given as

$$\frac{\partial F}{\partial t} + \frac{\partial \dot{x} F}{\partial x} = S_{in} + S_{nl} + S_{ds} , \tag{48}$$

23

where S_{in} is the wind input source term, S_{nl} represents nonlinear resonant wave-wave interactions and S_{ds} represents dissipative processes ('whitecapping'). Formally the first term of this equation can be omitted, since fetch-limited wave growth represents a steady problem. However, in a general purpose wave model the steady state is reached by calculating forward in time with a constant wind speed and direction until a steady state is obtained. In the present tests, the source terms of the original WAM model will be used (WAMDIG 1988); i.e., an input source term based on Snyder et al. (1981), the discrete interaction approximation of Hasselmann et al. (1985) to describe the the nonlinear interactions, and the dissipation parameterization of Komen et al (1984).

All fetch-limited growth tests are performed with a constant wind speed at 10m height $u_{10} = 20$m/s. A fairly common spectral discretization with 24 discrete spectral direction and 25 discrete frequencies is used ($\Delta\theta = 15°$ and $f_{i+1} = 1.1f_i$, with frequencies ranging from 0.041-0.42Hz). This spectral discretization is adequate for the wind speed considered here (see Tolman 1992). The space and time steps are chosen to represent a regional model implementation, where fetch-limitations are expected to be important ($\Delta x = 25$km, $\Delta t = 15$min), with a maximum fetch of 625km (25 grid points). The initial conditions consist of a JONSWAP spectrum with a peak frequency of 0.25Hz and a wave height of 0.79m.

No exact solution is available for Eq. (48), due to the complexity of the nonlinear interactions. The 'exact' solution will therefore again be approximated using a high resolution model. In this model the spectral discretization remains unchanged, but the spatial and temporal resolutions are increased to $\Delta x = 2.5$km and $\Delta t = 1.5$min. With this resolution the choice of the propagation scheme becomes immaterial. The first order scheme has been used here to obtain the exact solution.

The resulting dependency of the wave height H_s on the fetch x after 4 days of model integration is shown for several propagation schemes in Fig. 28a. The first order scheme (dotted line) overestimates the exact solution (solid line). Most of the error is concentrated in the first offshore grid point, as discussed by Tolman (1992). The UQ scheme (dashed line), follows the exact solution closely, and hence shows a small but distinct improvement compared to the first order scheme. This is in contrast with the findings of Tolman (1992), who showed no improvement when changing from the first order scheme to a second order accurate SHASTA scheme. This can be explained as

24

the latter scheme used a purely first order approach in the first grid point, whereas the UQ scheme uses a mixed first-order/third-order approach in the first grid point. The SHASTA scheme furthermore required some additional diffusion when combined with source terms, which may also be detrimental to the behavior of this scheme.

The UQ scheme results in a small oscillation of the solution in the steady regime, as observed in Fig. 28b (dashed lines). However, the solutions remain stable, and the oscillation are insignificant for most applications. If these oscillations are nevertheless unacceptable, they can be suppressed using a small, controlled amount of diffusion. Considering that diffusion already is an integral part of the UQDC scheme, this diffusion is modeled explicitly. To assure that the diffusion is small for all wave components, the diffusion is defined using a preset cell-Reynolds (or cell-Peclet) number $\mathcal{R} = c_g \Delta x D_g^{-1}$, where D_g represents the diffusion for growing wave components. Note that large values of $\mathcal{R}$ represent conditions with small diffusion. Applying the corresponding diffusion isotropically, we obtain

$$D_g = D_{ss} = D_{nn} = \frac{c_g \, \min(\Delta x, \Delta y)}{\mathcal{R}} \, . \tag{49}$$

Results for the UQ scheme with a diffusion defined by $\mathcal{R} = 10$ are shown in Fig. 28 (chain line). This small amount of diffusion removes virtually all oscillations. The resulting growth curves show a minor influence from diffusion for the first few grid points (compare chain and dashed lines), but effects of this diffusion on the growth behavior are generally negligible.

For practical applications, the diffusion defined by Eq. (49) should be incorporated in the UQDC scheme. This requires the combination of the diffusion terms contained in Eqs. (33), (34) and (49). The wave age $U_{10}c^{-1} = U_{10}k\sigma^{-1}$ is a natural parameter to identify (potentially) growing wave components. Requiring that the propagation diffusion of Eqs. (33) and (34) is used for $U_{10}c^{-1} < 0.7$, and that the growth diffusion of Eq. (49) is used for $U_{10}c^{-1} > 1.0$, the final diffusion tensor is defined as

$$X_g = \min\left\{ 1 \, , \, \max\left[0 \, , \, 3.3\left(\frac{k\,U_{10}}{\sigma}\right) - 2.3 \right] \right\} \, , \tag{50}$$

$$D_{ss} = X_g D_g + (1 - X_g)(\Delta c_g)^2 \, T_s/12 \, , \tag{51}$$

25

$$D_{nn} = X_g D_g + (1 - X_g)(c_g \Delta \theta)^2 \, T_s / 12 \,. \tag{52}$$

The UQDC scheme with this diffusion correction gives practically identical results to the UQ scheme with the diffusion of Eq. (49) (chain line in Fig. 28).

7 Discussion and conclusions

This report evaluates several propagation schemes for ocean wind wave models. It is based on previous experience in wave modeling and modeling of pollution transport, and does not present new numerical methods. A review of available methods suggests that explicit finite difference schemes are prime candidates to be used in wave models. Implicit FD schemes and semi-Lagrangian schemes are also potentially useful. The application of the latter two schemes is discussed in more detail below. Based on previous experience in the field of pollution models, the third-order accurate ULTIMATE QUICK-EST (UQ) scheme was selected. This scheme was shown to be sufficiently accurate to produce the so-called garden sprinkler effect (GSE), where the initially continuous wave field disintegrates into a set of discrete wave fields. This effect is solely due to the poor resolution of spectral directions, and is therefore not an artifact of the UQ scheme. It is expected to occur with any accurate propagation scheme. This problem can be avoided if the directional resolution of the spectrum is increased by an order of magnitude. However, for most wave models this is not economically feasible.

An alternate solution to avoid the GSE is the inclusion of a diffusive dispersion correction, as suggested by Booij and Holthuijsen (1987) (denoted as the UQDC scheme). This approach effectively removes the garden-sprinkler effect. Furthermore, simplifications to this approach as suggested by Booij and Holthuijsen proved to be viable. For idealized swell propagation tests the UQ scheme performs far better than the first order scheme. However, it should be noted that the diffusive correction of Booij and Holthuijsen introduces some non-physical aspects into the model. Swell shows an increasingly narrower directional distribution during propagation. This implies that swell produces a sharp shadow zone behind islands. This can be observed in the 'exact' swell model of Fig. 4d, where the swell field is cut-off by New Guinea. In contrast, the diffusive correction shows enhanced (lateral) diffusion with

26

increasing swell age T_s in Eqs. (33) and (34). If the UQ scheme is used in combination with this diffusive correction (Figs 12d and 15d), the transition to a shadow zone behind islands will be smoothed significantly.

If the wave spectrum is considered to be continuous in direction and frequency, both directional and frequency dispersion occur. Frequency dispersion is poorly described when using conventional spectral resolutions in combination with a peaked initial spectrum. This poor behavior is related to the frequency resolution of the model. Contrary to common belief, the conventional 10% resolution of the spectral frequencies is thus inadequate for the peaked spectrum considered here. Adopting a smoother initial spectrum and a 5% frequency resolution improves frequency dispersion dramatically. For such conditions the spatial distribution of wave heights and the maximum wave height become fairly insensitive to the choice of the propagation scheme. The first order scheme does, however, have a tendency to generate spurious maxima for southward (or northward) travelling wave components. Whereas overall wave heights are only slightly influenced by the propagation scheme, local spectra show larger differences. As an example, it is shown that the peak frequency is much more accurately described by the UQDC scheme. The UQDC scheme furthermore shows a more consistent temporal (and hence spatial) evolution of wave spectra. The latter differences will be important for swell prediction, in particular for offshore operations, where dynamical responses of offshore equipment to wave motion are strongly governed by the wave frequency. It might also allow for decomposing the wave field in discrete swell fields, the origin of which can be retrieved without calculating the local swell age T_s. This might be useful in data assimilation schemes.

Both the first order and UQDC schemes interact well with source terms. Unlike in previous attempts to use a higher order scheme (Tolman 1992), additional diffusion is not required to stabilize fetch-limited growth behavior for the UQDC scheme. It is shown that the UQDC scheme results in slightly more accurate fetch-limited growth. However, as was concluded before (Tolman 1992), effects of the propagation scheme on fetch-limited growth behavior are minor.

Considering the above, the UQDC scheme presents a significant improvement over the first order scheme. Its main advantages are that it does not produce spurious maxima related to southward (northward) travelling wave components, and that it results in a more consistent temporal and spatial evolution of the wave field. The latter is particularly important for consis-

tent swell prediction, and might have implications for data assimilation. It remains to be seen if the effects on local wave height are significant. This depends largely on the actual frequency spectra of the wind sea field generating the swell, and on spectral transformations during the transition from wind sea to swell. Considering that Figs. 25a and 25b represent limiting cases for narrow and wide spectra, differences between maximum wave height of 10 to 20% might be expected.

Even after the selection of a better numerical scheme, there is always room to make further improvements to the numerics of a model. First, spatial wave propagation essentially represents one-dimensional propagation in a two- or three-dimensional space (longitude-latitude(-direction)). In the present approach, propagation in each space is treated separately. It might be more economical and more accurate to treat this propagation as truly one-dimensional. In a finite difference approach this is possible, but requires additional cross-terms which complicate the scheme . A more natural way of treating the propagation as one-dimensional would be a semi-Lagrangian approach. Secondly, wave models require high resolution mostly near coast lines and to describe details of the bathymetry, but generally not in the deeper ocean. It might therefore be a significant improvement if the wave model is formulated in terms of a variable grid. Thirdly, with increased resolution, the time steps required by explicit finite difference schemes become continually smaller. To avoid this, implicit or semi-Lagrangian schemes could be adopted. If necessary, such approaches can be adopted in selected spaces only. For instance, propagation in direction space due to refraction is known to pose serious stability problems in shallow water wave models, and is therefore could be treated with an implicit scheme. In view of the above, much numerical development work can still be done with respect to wave modeling.

28

<center>REFERENCES</center>

Booij, N. and L.H. Holthuijsen, 1987: Propagation of ocean waves in discrete spectral wave models. *J. Comput. Phys.*, **68**, 307-326.

Cahyono, 1994: Three-dimensional numerical modelling of sediment transport processes in non-stratified estuarine and coastal waters, PhD thesis, University of Bradford, 315 pp.

Davis, R.W., and E.F. More, 1982: A Numerical study of vortex shedding from rectangles. *J. Fluid Mech.*, **116** 475-506.

Falconer, R.A., and Cahyono, 1993; Water quality modelling in well mixed estuaries using higher order accurate differencing schemes. Advances in hydroscience and engineering, S.S.Y. Wang Ed., 81-92.

Fletcher, C.A.J., 1988: *Computational techniques for fluid dynamics, part I and II.* Springer, 409+484 pp.

Gelci, R., H. Cazalé and J. Vasal, 1956: Utilization des diagrammes de propagation à la prévision énergétique de la houle. *Bulletin d'information du commité central d'oceanographie et d'etudes des côtes*, **8**, 169-197.

Groves, G.W., and J. Melcer, 1961: On the propagation of ocean waves on a sphere. *Geof. Int.*, **8**, 77-93.

Hasselmann, D.E., M. Dunckel and J.A. Ewing, 1980: Directional wave spectra observed during JONSWAP *J. Phys. Oceanogr.*, **11**, 1264-1280.

Hasselmann, K., T.P. Barnett, E. Bouws, H. Carlson, D.E. Cartwright, K. Enke, J.A. Ewing, H. Gienapp, D.E. Hasselmann, P. Kruseman, A. Meerburg, P. Müller, D.J. Olbers, K. Richter, W. Sell and H. Walden, 1973: Measurements of wind-wave growth and swell decay during the Joint North Sea Wave Project (JONSWAP). *Ergänzungsheft zur Deutschen Hydrographischen Zeitschrift*, Reihe A (8) Nr. 12, 95 pp.

Hasselmann, S., K. Hasselmann, J.H. Allender and T.P. Barnett, 1985: Computations and parameterizations of the nonlinear energy transfer in a gravity-wave spectrum, Part II: Parameterizations of the nonlinear energy transfer for application in wave models. *J.Phys. Oceanogr.*, **15**, 1378-1391.

Holthuijsen, L.H., and H.L. Tolman, 1991: Effects of the Gulf Stream on ocean waves. *J. Geophys. Res.*, **96**, 12755-12771.

Komen, G.J., S. Hasselmann and K. Hasselmann, 1984: On the existence of a fully developed wind-sea spectrum. *J. Phys. Oceanogr.*, **14**, 1271-1285.

<center>29</center>

————, L. Cavaleri, M. Donelan, K. Hasselmann, S. Hasselmann and P.E.A.M. Janssen, 1994: *Dynamics and modelling of ocean waves.* Cambridge university press, 532 pp.

Leonard, B.P., 1979: A stable and accurate convective modelling procedure based on quadratic upstream interpolation. *Comput. Methods Appl. Mech. Engng*, **18**, 59-98.

————, 1991: The ULTIMATE conservative difference scheme applied to unsteady one-dimensional advection. *Comput. Methods Appl. Mech. Engng*, **88**, 17-74.

Mei, C.C., 1983: *The applied dynamics of ocean surface waves.* Wiley, New York, 740 pp.

Neu, W.L., and Y.S. Won, 1990: Propagation schemes for wind wave models with finite depth and current. it Ocean wave mechanics, computational fluid dynamics and mathematical modelling. M. Rahman, Ed. 947-954.

Peregrine, D.H., and I.G. Jonsson, 1983: *Interaction of waves and currents.* Miscellaneous report no. 83-6. CERC, US Army Corps of Engineers.

Snodgrass, F.E. et al., 1966: Propagation of ocean swell across the pacific. *Phil. Trans. Roy. Soc. A*, **259**, 431-497.

Snyder, R.L., F.W. Dobson , J.A. Elliott and R.B. Long, 1981: Array measurements of atmospheric pressure fluctuations above surface gravity waves. *J. Fluid Mech.*, **102**, 1-59.

SWAMP group, 1985: *Ocean wave modelling.* Plenum Press, 256 pp.

SWIM group, 1985: A shallow water intercomparison of three numerical wave prediction models SWIM. *quart. J. Roy. Meteor. Soc.*, **111**, 1087-1112.

Tolman, H.L., 1991: A third-generation model for wind waves on slowly varying, unsteady and inhomogeneous depths and currents. *J. Phys. Oceanogr.*, **21**, 782-797.

————, 1992: Effects of numerics on the physics in a third-generation windwave model. *J. Phys. Oceanogr.*, **22**, 1095-1111.

WAMDIG, 1988: The WAMmodel - a third generation ocean wave prediction model. *J. Phys. Oceanogr.*, **18**, 1775-1810.

Whitham, G.B., 1974: *Linear and nonlinear waves.* Wiley, 636 pp.

Yanenko, N.N., 1971: *The method of fractional steps.* Springer, Berlin, 160 pp.

Figure captions

Fig. 1   One-dimensional propagation tests. dotted lines : exact solution,
         dashed lines : first order scheme, solid lines : UQ scheme. (a) Similar
         to test of Tolman (1992), Fig. 6., 100 time steps with $C = 0.28$ (b) –
         (d) propagation around the globe of wave energy distributions with
         different spatial extends. Wave period $T = 24.9$s, grid increment
         $\Delta x = 1°$, time step $\Delta t = 1$h, 576 time steps.

Fig. 2   Two-dimensional swell propagation in deep water. (a) Initial Gaus-
         sian wave height distribution, with a spread of $2\Delta x$ and $2\Delta y$ in
         the two spaces. (b) – (e) Propagation after 60 time steps with
         $c_g\Delta t/\Delta x = c_g\Delta t/\Delta y = 0.63$. First order scheme with $\theta = 0°$ (panel
         b) and $\theta = 45°$ (panel c). UQ scheme with $\theta = 0°$ (panel d) and
         $\theta = 45°$ (panel e). Contour intervals at 10% of the initial maximum
         wave height. + indicates the expected location of the maximum
         wave height.

Fig. 3   Swell heights after 0, 2, 4 and 6 days (panels a through d) for the
         North Pacific swell propagation test with $\bar{\theta} = 120°$ initially (Mer-
         cator projection). Contours at 10% of the initial maximum wave
         height in panel a) and at 5% in panels b) through d). 'Exact' solu-
         tion obtained with the UQ scheme with $\Delta\lambda = \Delta\phi = 0.25°$, $\Delta\theta = 2.5°$
         and $\Delta t = 10$min.

Fig. 4   Like Fig. 3 with $\bar{\theta} = 150°$ initially.

Fig. 5   Maximum wave height as a function of time in the North Pacific
         propagation test, normalized with the initial maximum wave height.
         dotted line : based on Eq. (26); solid lines : 'exact' solution; chain
         lines : first order scheme; dashed lines : UQ scheme. (a) linear
         scaling. (b) logarithmic scaling.

Fig. 6   Like Fig. 3 for the first order scheme using a realistic model resolution
         ($\Delta\lambda = 1.25°$, $\Delta\phi = 1°$, $\Delta\theta = 15°$ and $\Delta t = 20$min). Initial $\bar{\theta} = 120°$.

Fig. 7   Like Fig. 6. Initial $\bar{\theta} = 150°$.

Fig. 20   Like Fig. 17 for the UQDC scheme with constant swell age $T_s = 5$ days.

Fig. 21   Maximum wave height as a function of time in the full spectral North Pacific propagation tests, normalized with the initial maximum wave height. Initial conditions consists of a JONSWAP spectrum wit a conventional frequency resolution (Fig. 16a). dotted line : expected dispersion behavior based on Eq. (44); dashed line : first order scheme; double chain line : UQ scheme; chain line : UQDC scheme with dynamic T_s; solid line : UQDC scheme with $T_s = 5$days. (a) linear scaling. (b) logarithmic scaling.

Fig. 22   Like Fig. 17, Pierson-Moskowitz spectrum with enhanced frequency resolution.

Fig. 23   Like Fig. 20, Pierson-Moskowitz spectrum with enhanced frequency resolution.

Fig. 24   Like Fig. 21, Pierson-Moskowitz spectrum with enhanced frequency resolution.

Fig. 25   The significant wave height normalized with the initial maximum wave height at 160°W 20°N as a function of time according to the first order scheme (dotted lines) and the UQDC scheme with constant swell age $T_s = 5$ days (solid lines) (a) Conventional frequency resolution, JONSWAP spectrum (corresponds to Figs. 16a, 17 and 20). (b) Enhanced frequency resolution, Pierson-Moskowitz spectrum (corresponds to Figs. 16b, 22 and 23).

Fig. 26   Like Fig. 25 for peak frequency. Dashed line represents expected peak frequency for point source.

Fig. 27   Like Fig. 25 for distance of swell source r as calculated form the temporal derivatives of the peak frequency. Dashed line: distance to center of source region.

Fig. 28   Growth curves for fetch-limited wave growth and a wind speed of 20m/s. (a) Wave height H_s as a function of the fetch x after 4 days of model integration. Wave height H_s as a function of time for three

fetches x. Solid lines : exact solution (high resolution model); dotted lines : first order scheme; dashed lines : UQ scheme; chain lines : UQ scheme with isotropic diffusion ($\mathcal{R} = 10$). $\Delta\theta = 15°$, $f_{i+1} = 1, 1 f_i$, $f_{\min} = 0.041$Hz, $f_{\max} = 0.42$Hz, $\Delta x = 25$km and $\Delta t = 15$min.

Fig. 1

Fig. 2

(a)

(b)

(c)

(d)
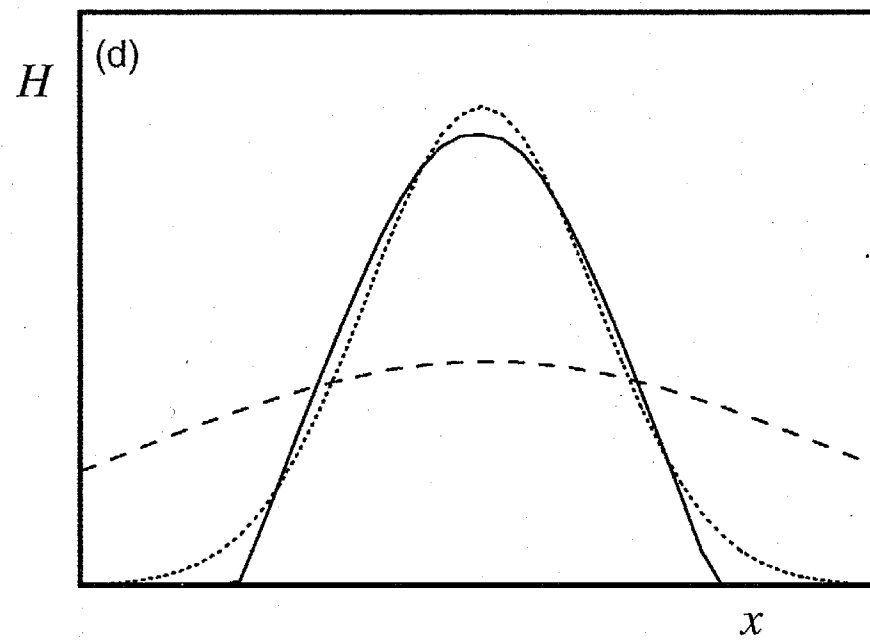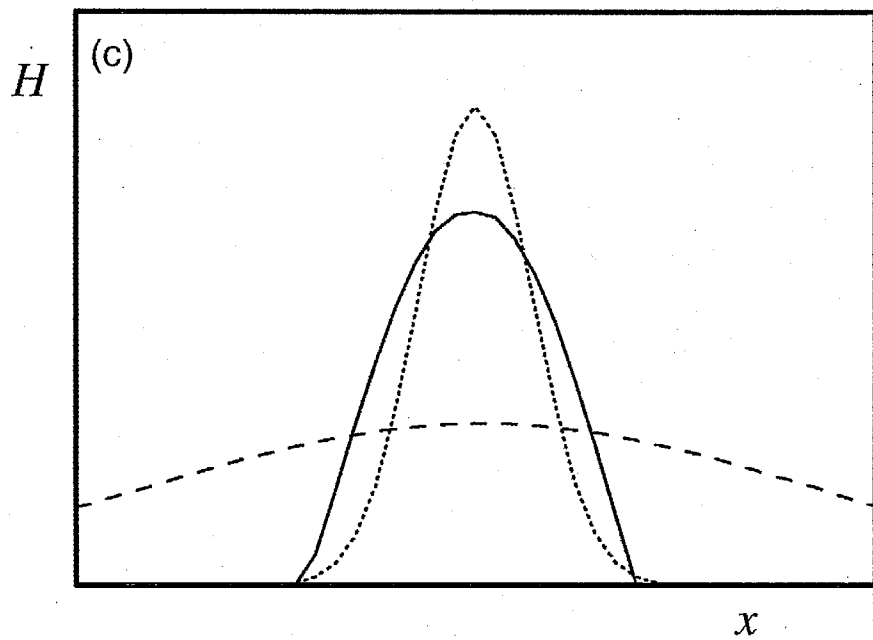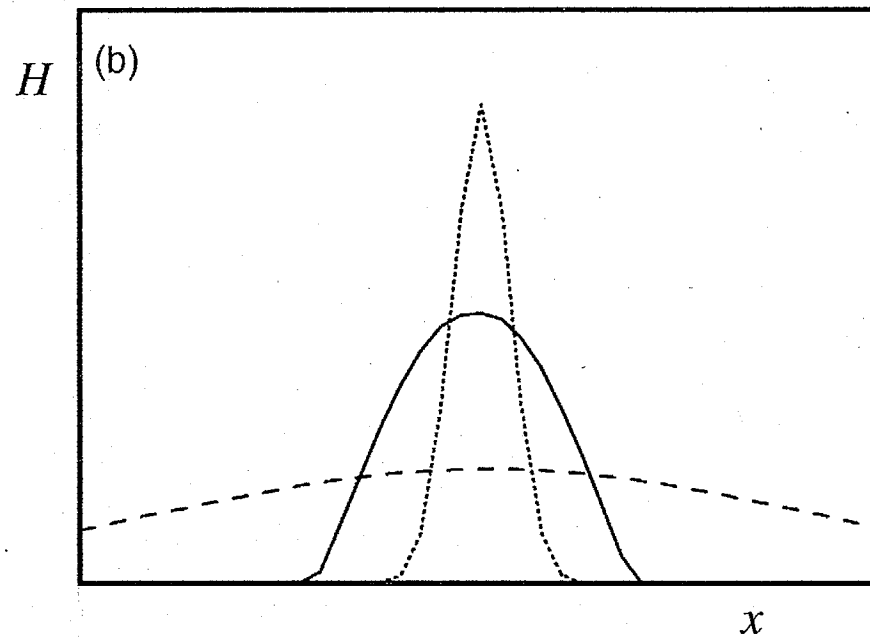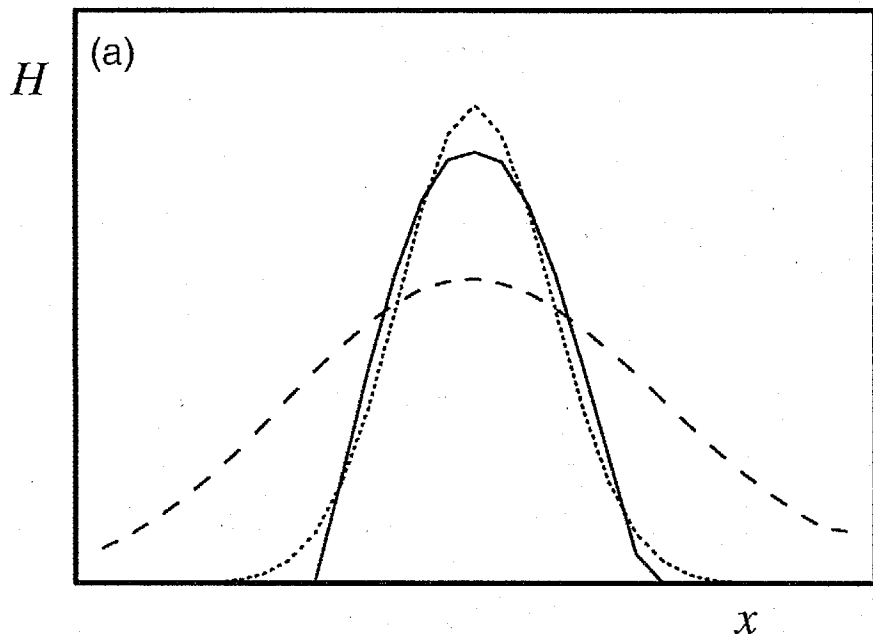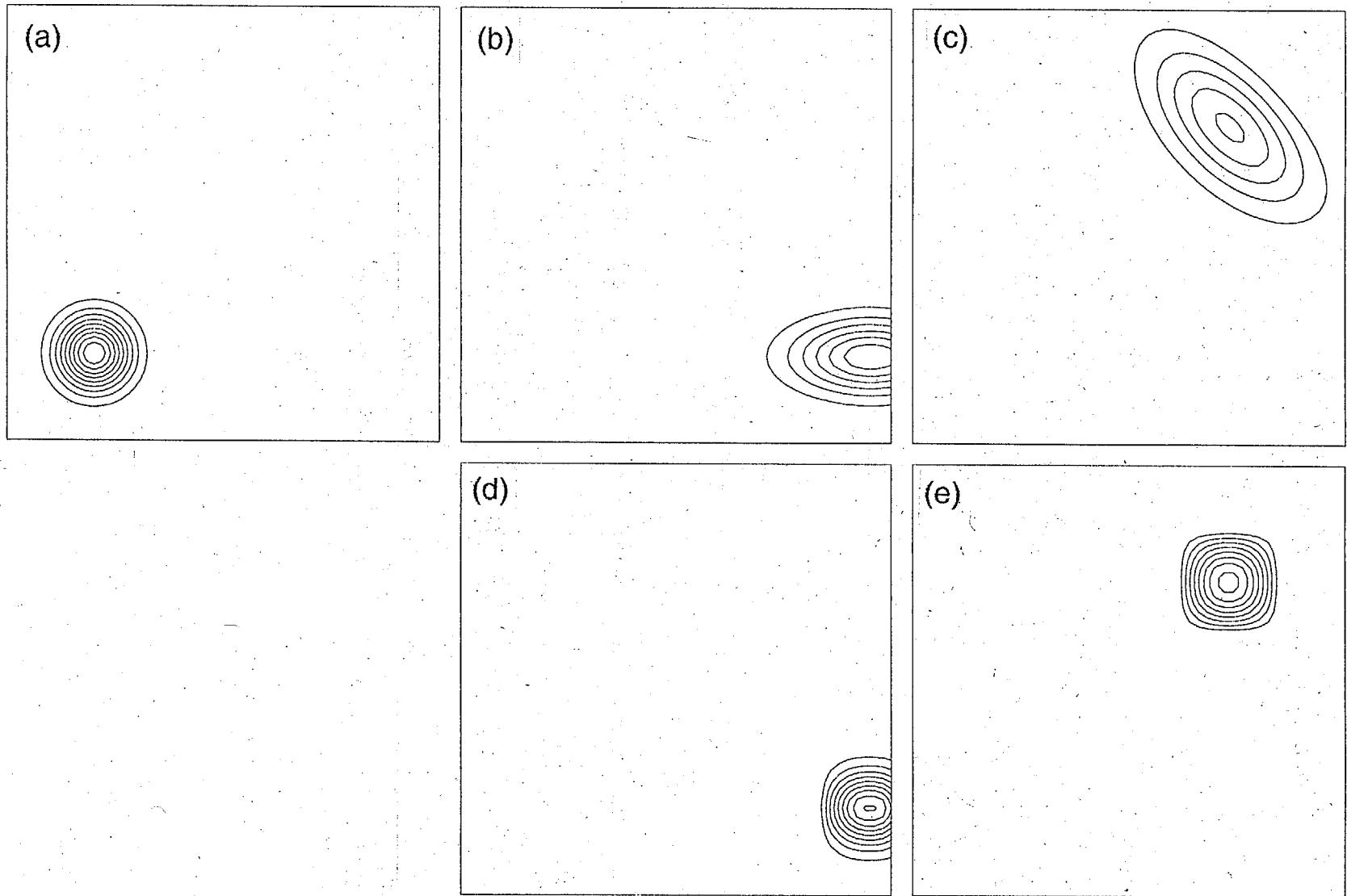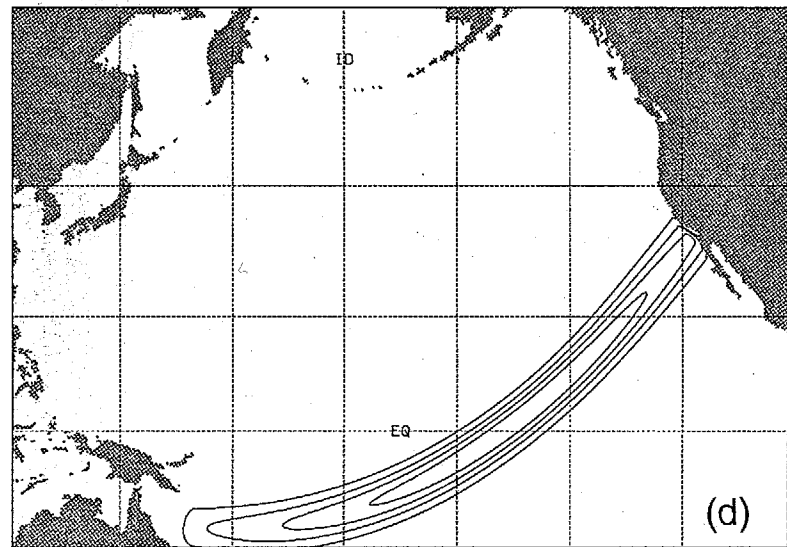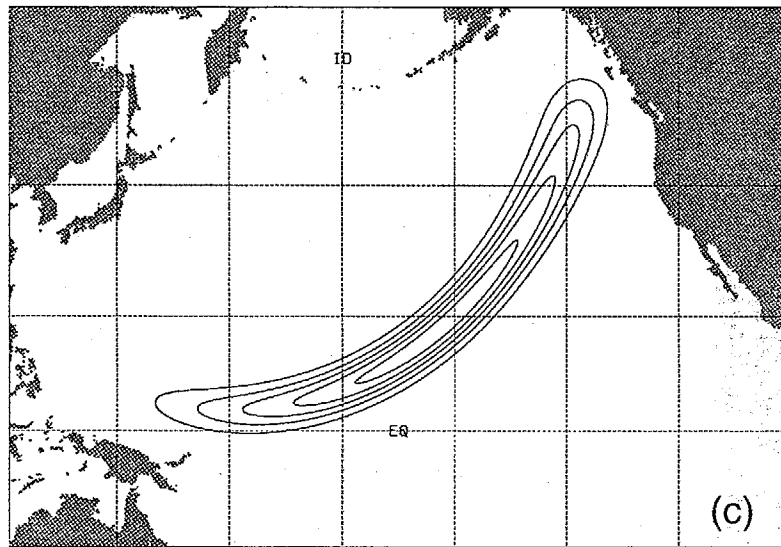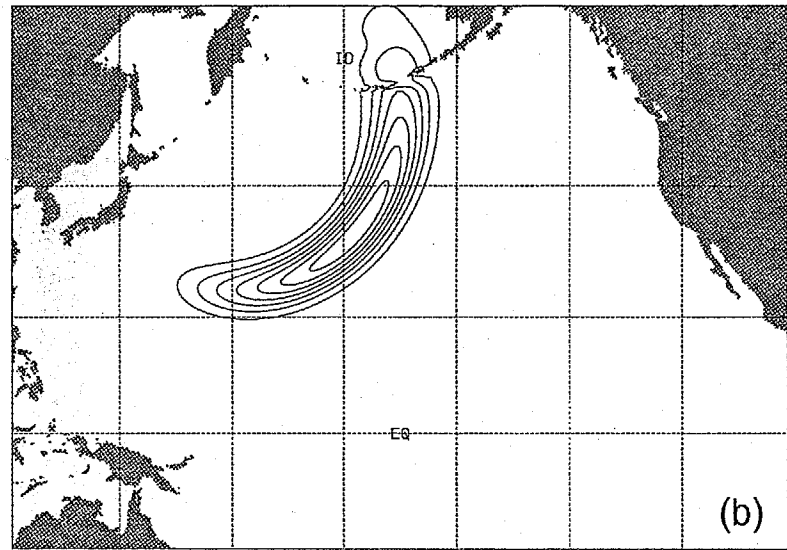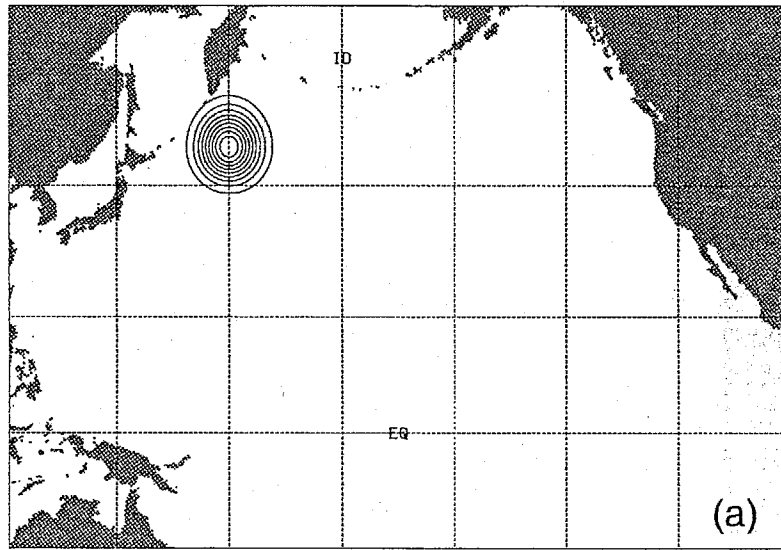
Fig. 3
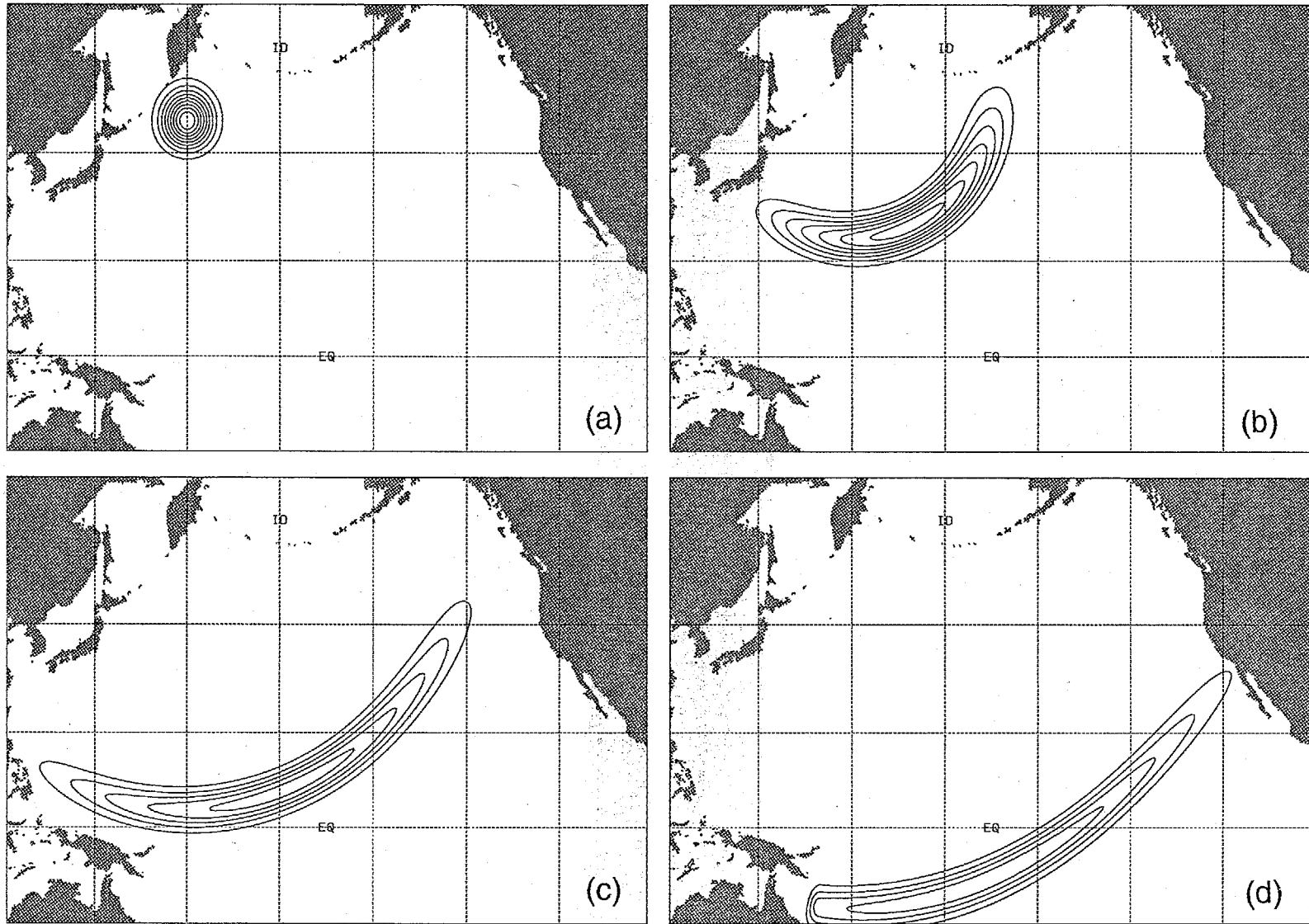
Fig. 4
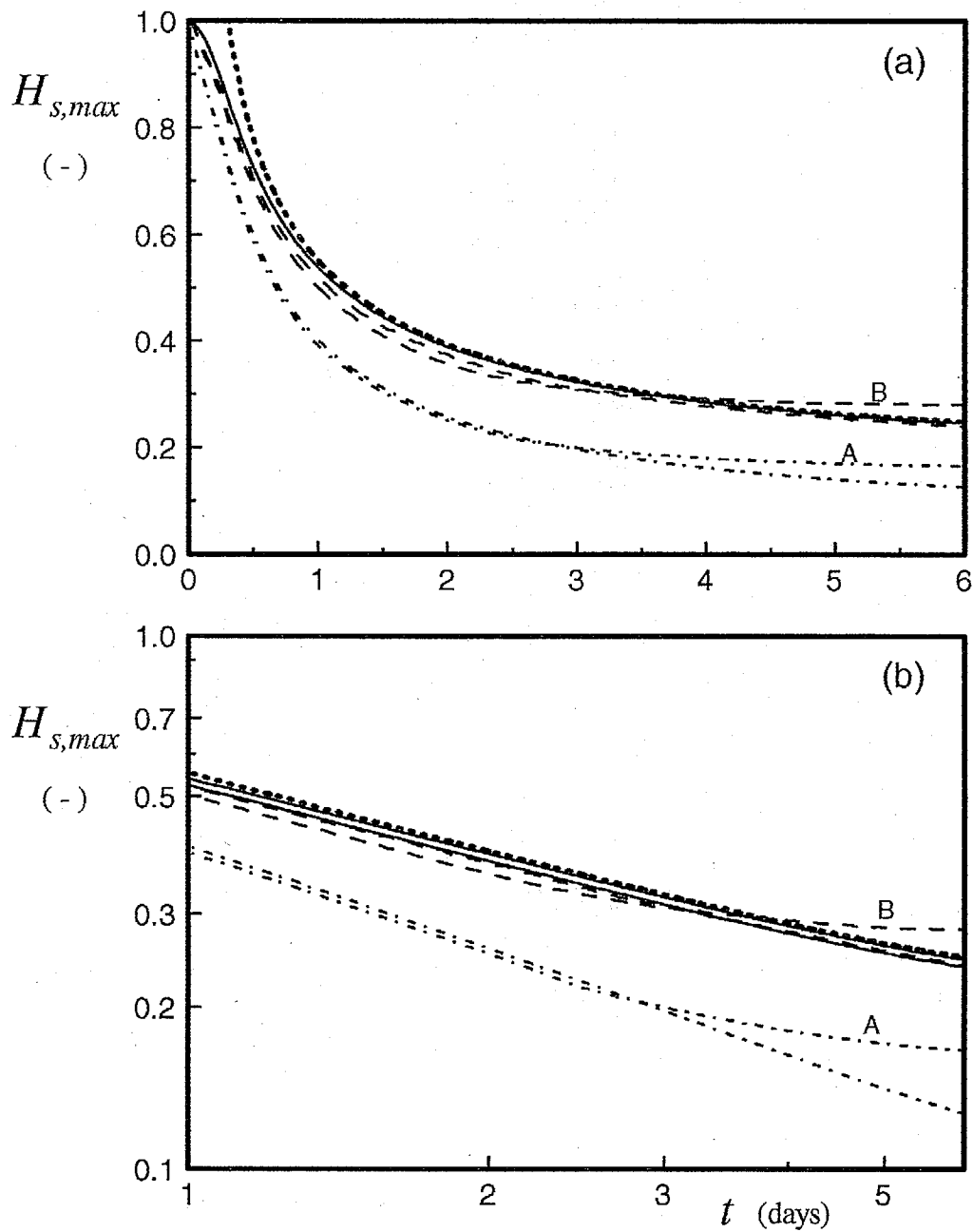
Fig. 5
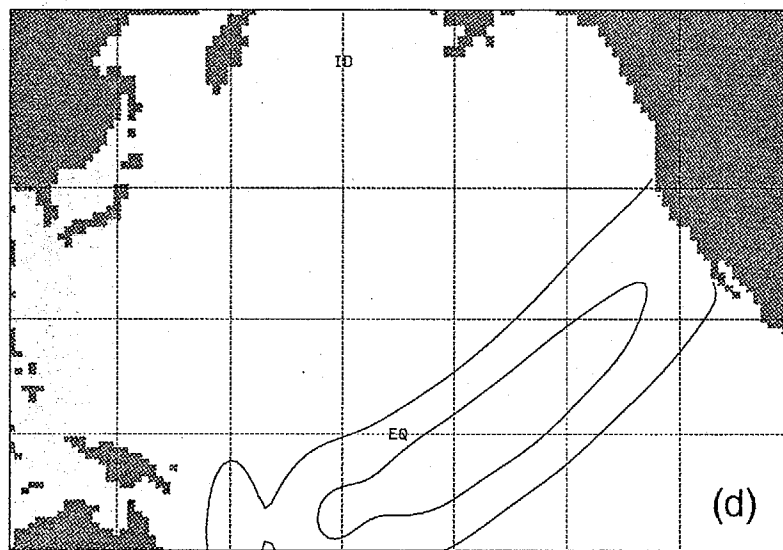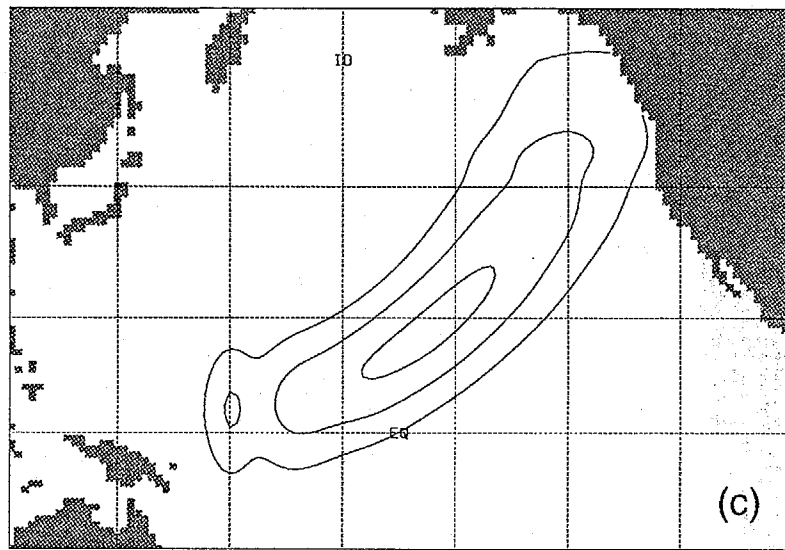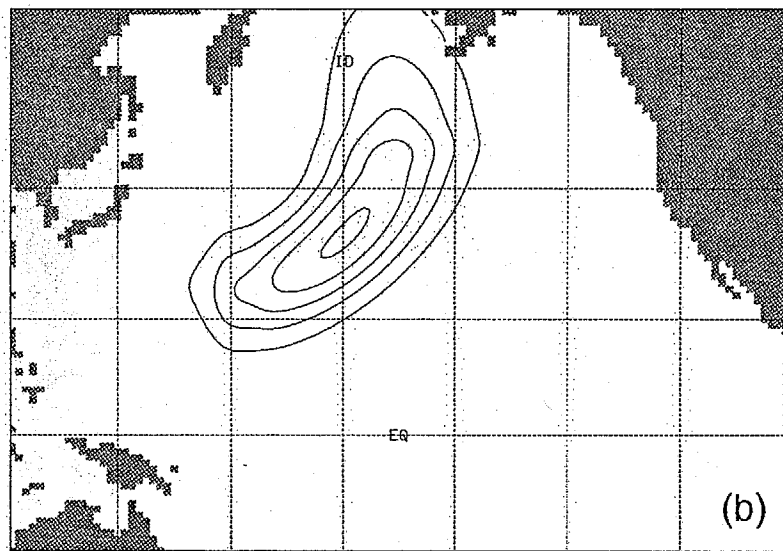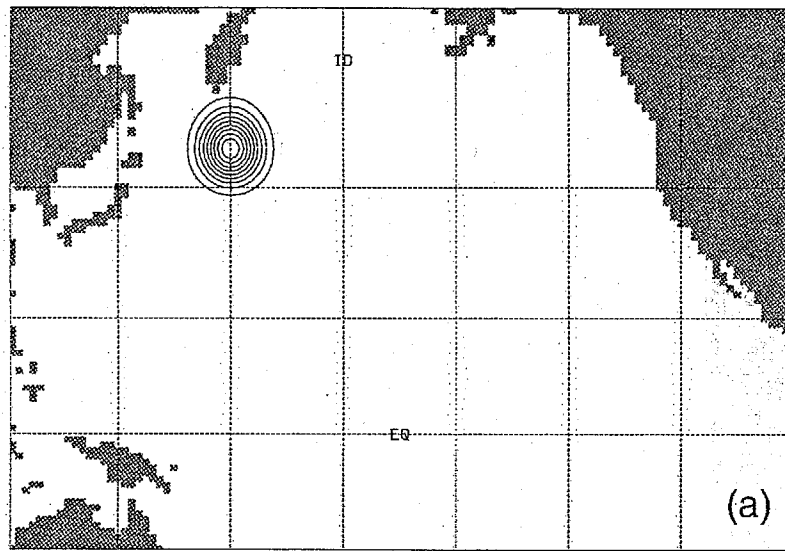
Fig. 6
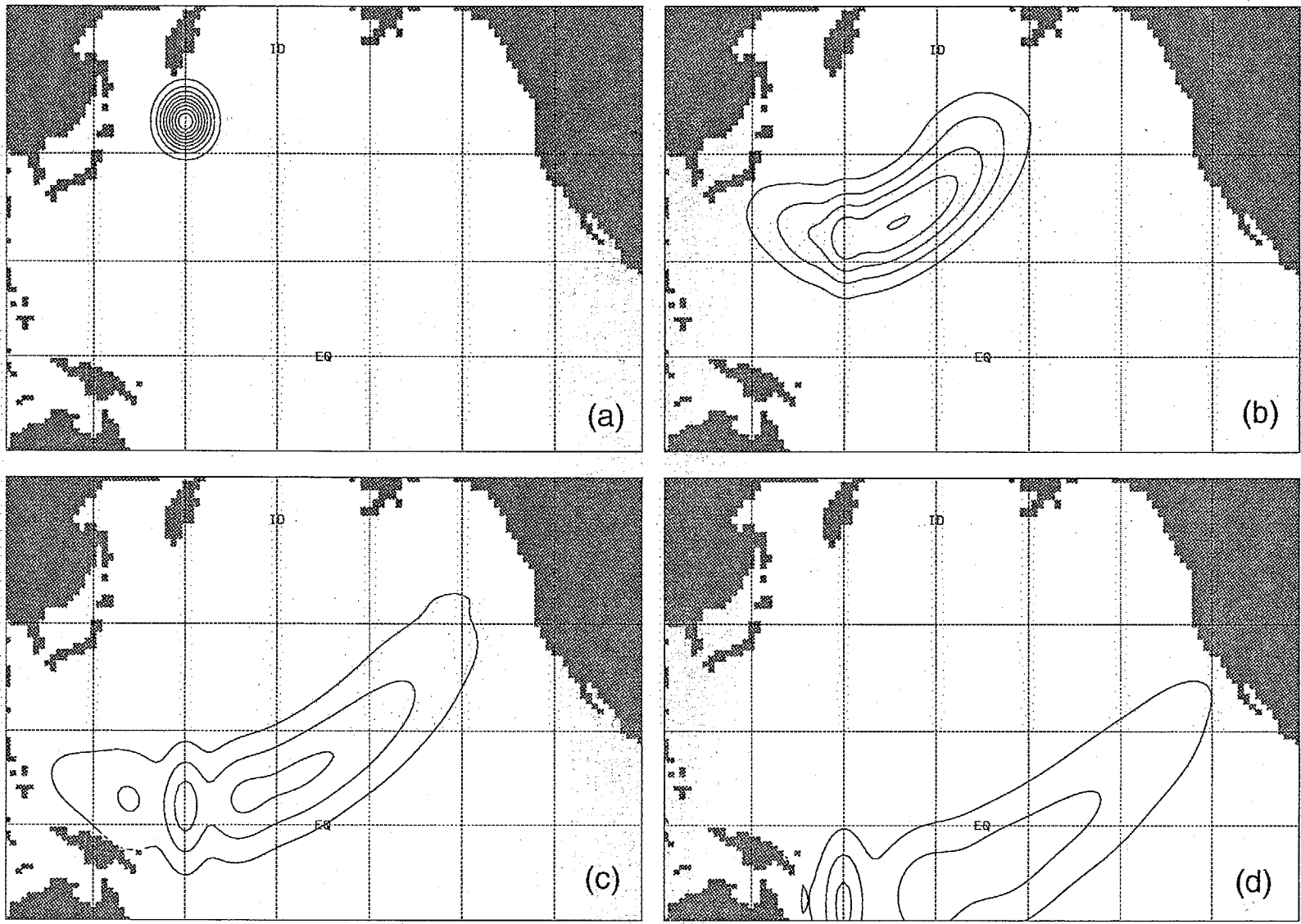
Fig. 7

Fig. 8

Fig. 9

Fig. 10

(a)

(b)

(c)

(d)

Fig. 11

Fig. 12

Fig. 13

(a) (b) (c) (d)
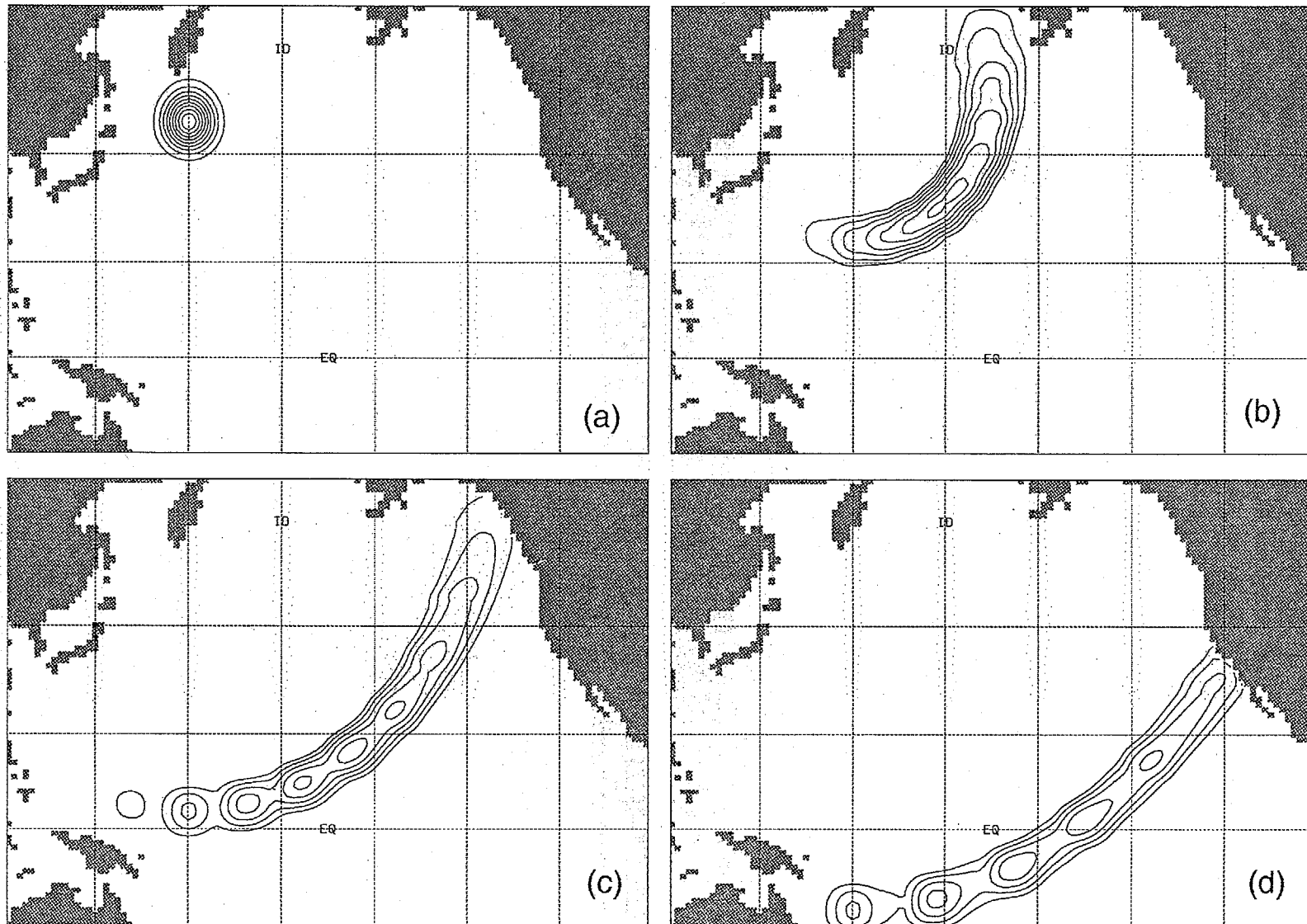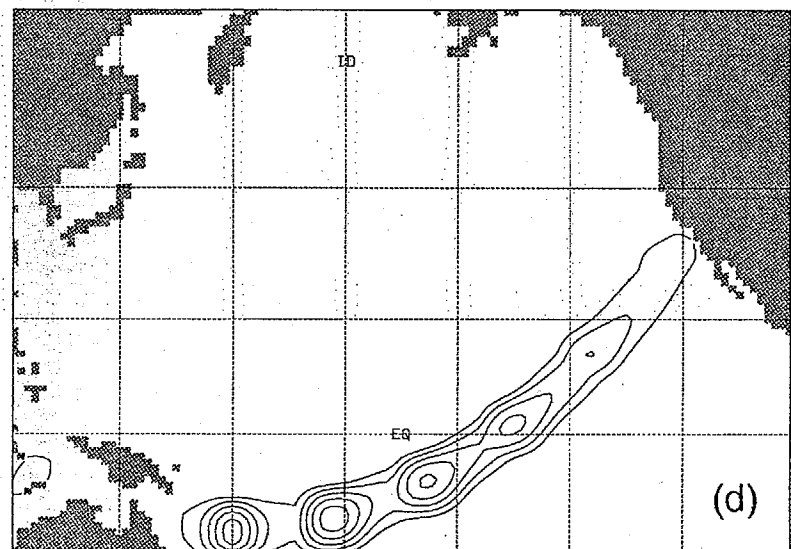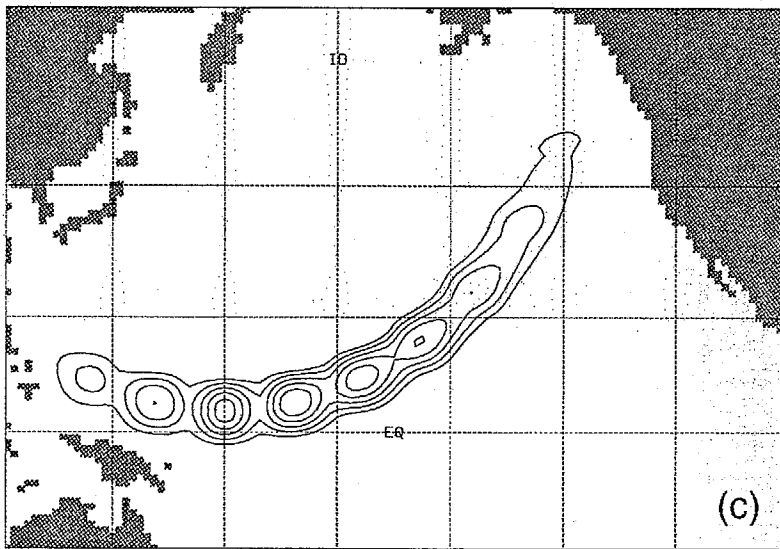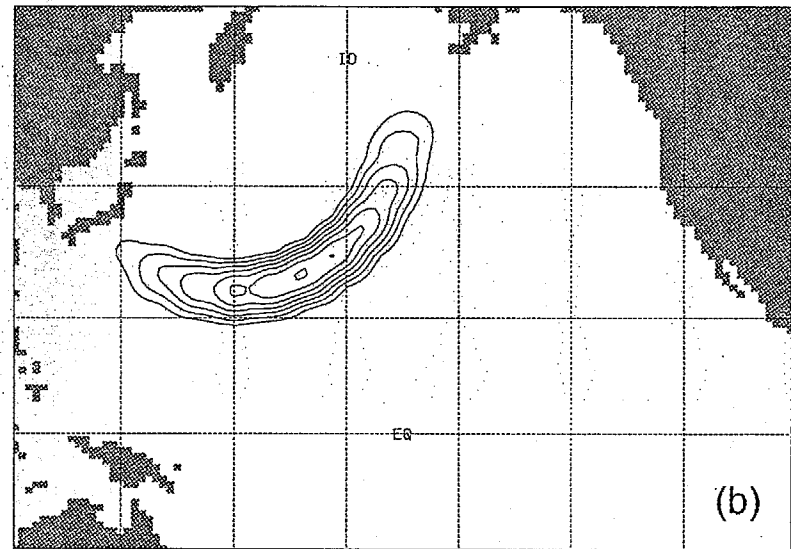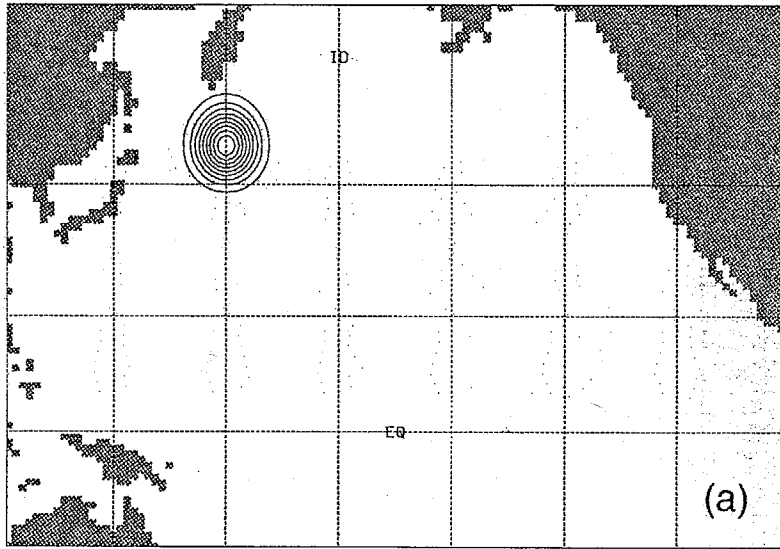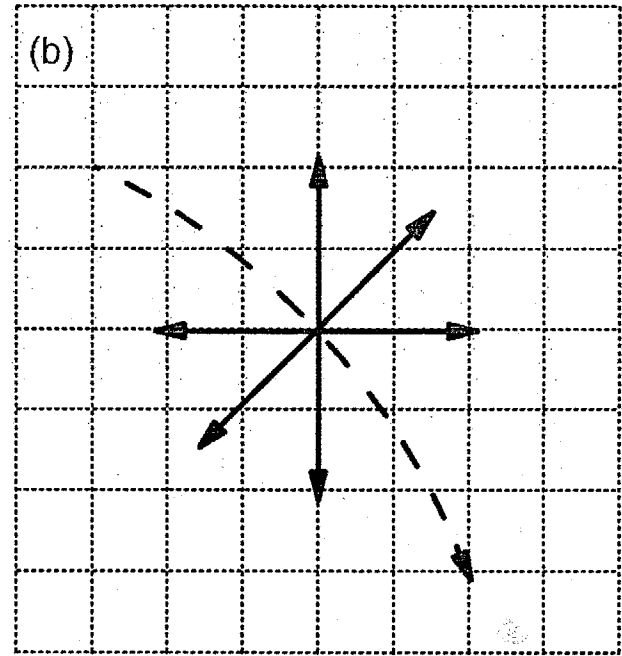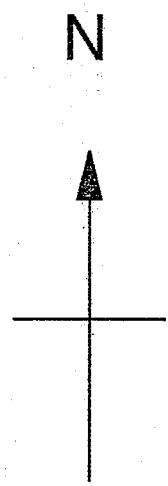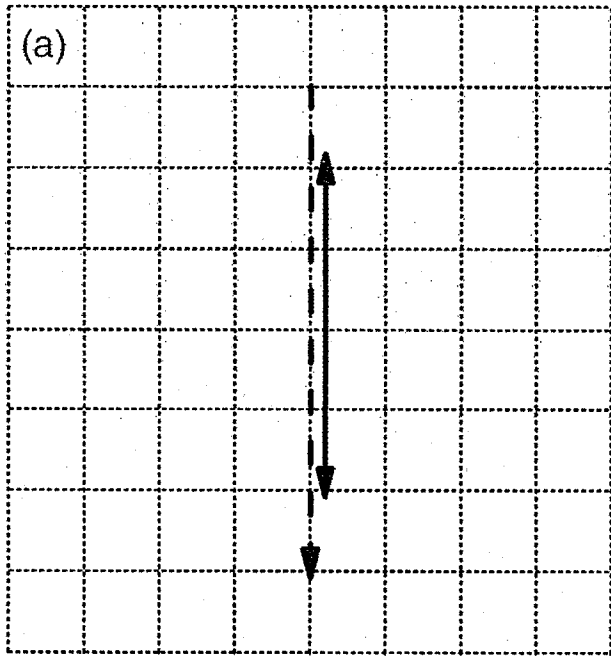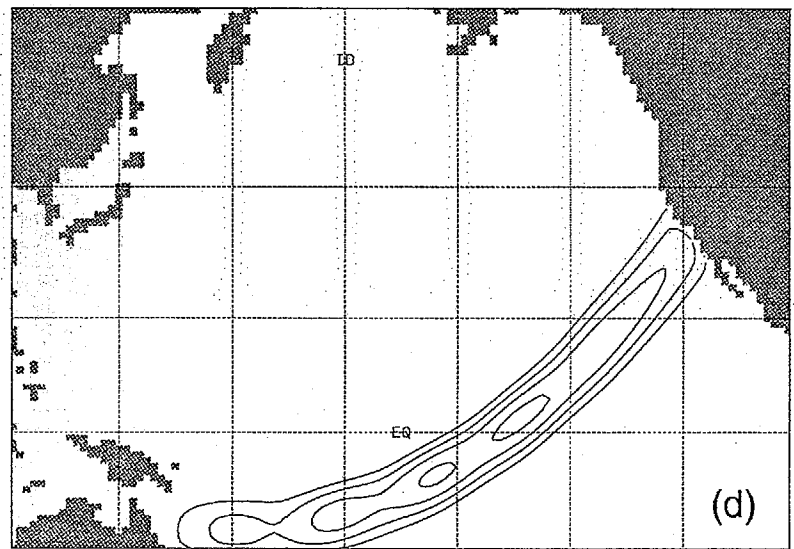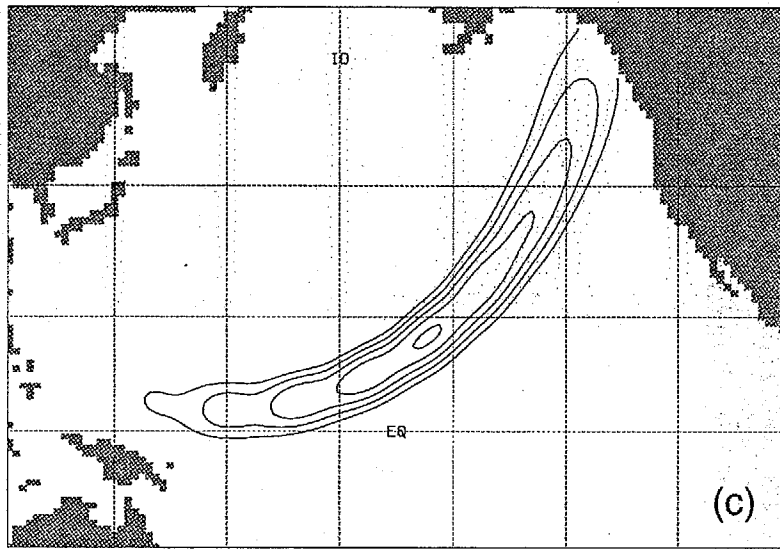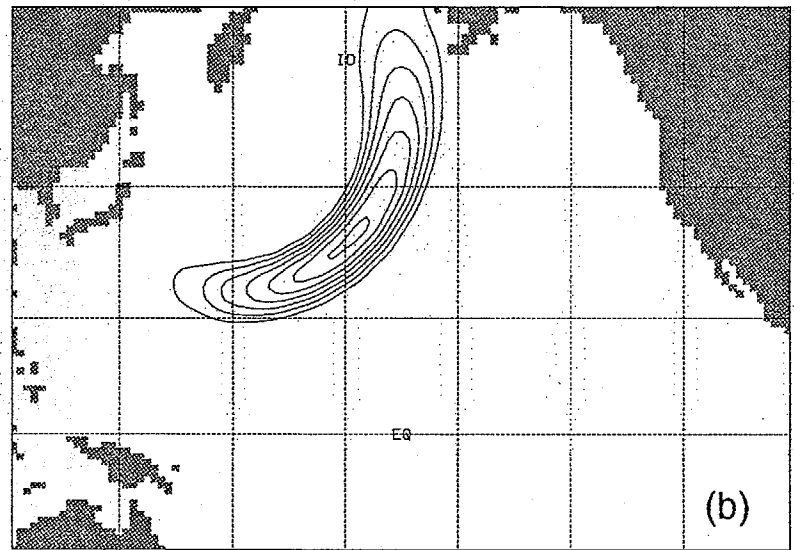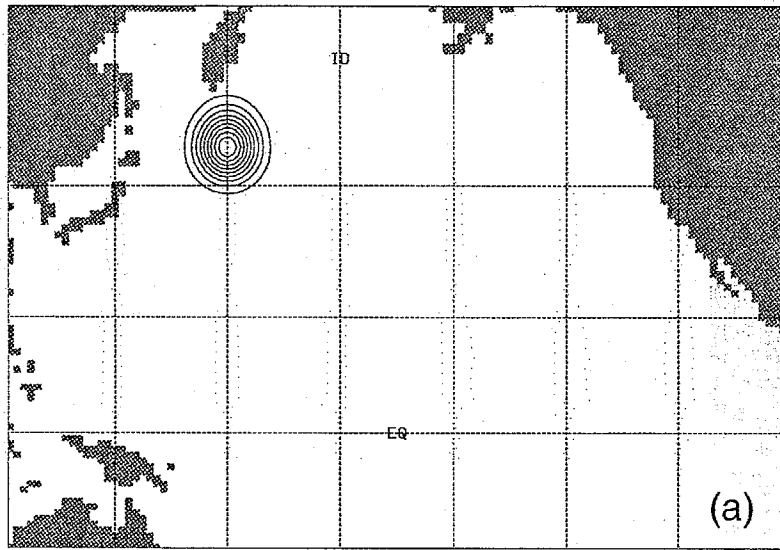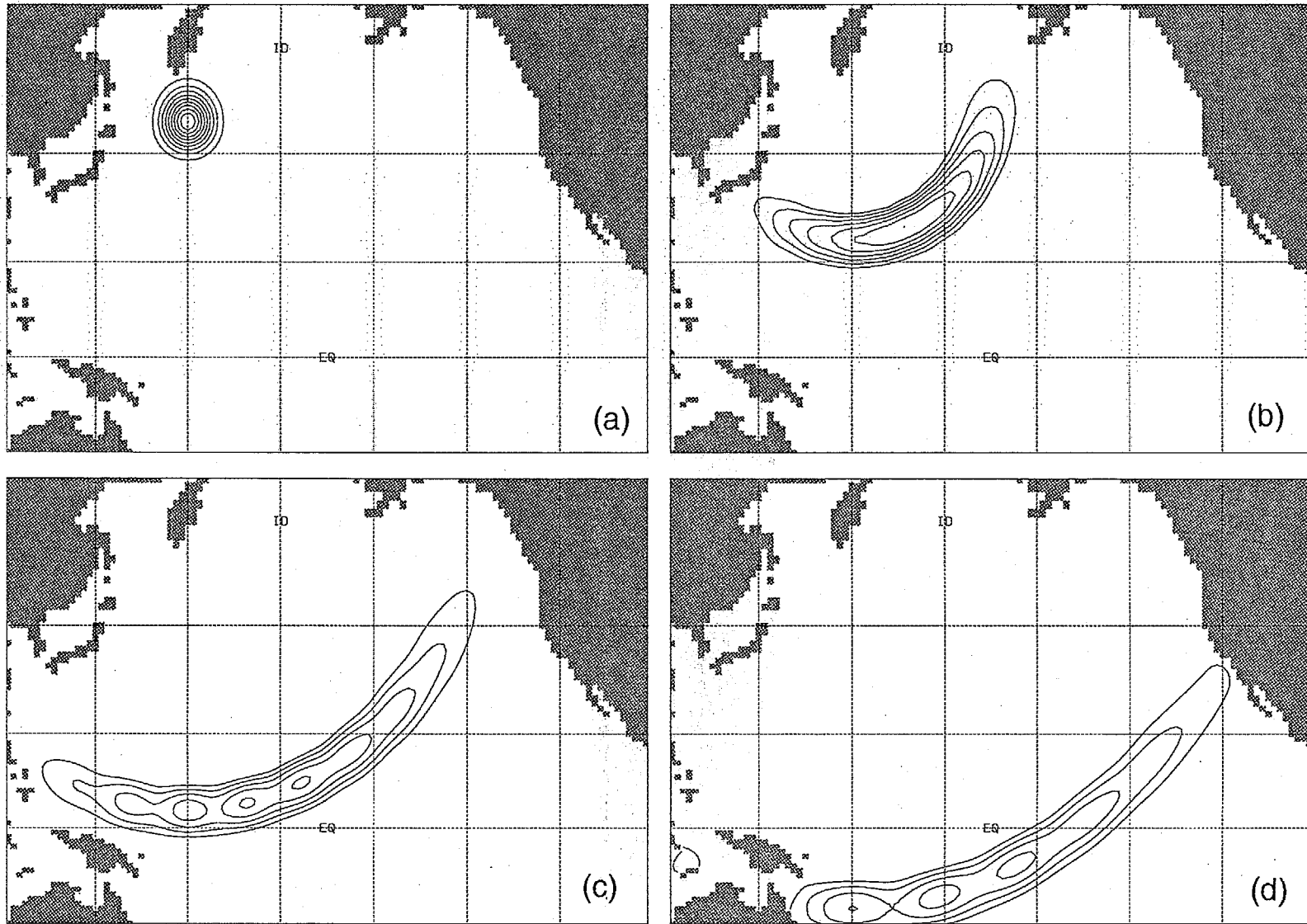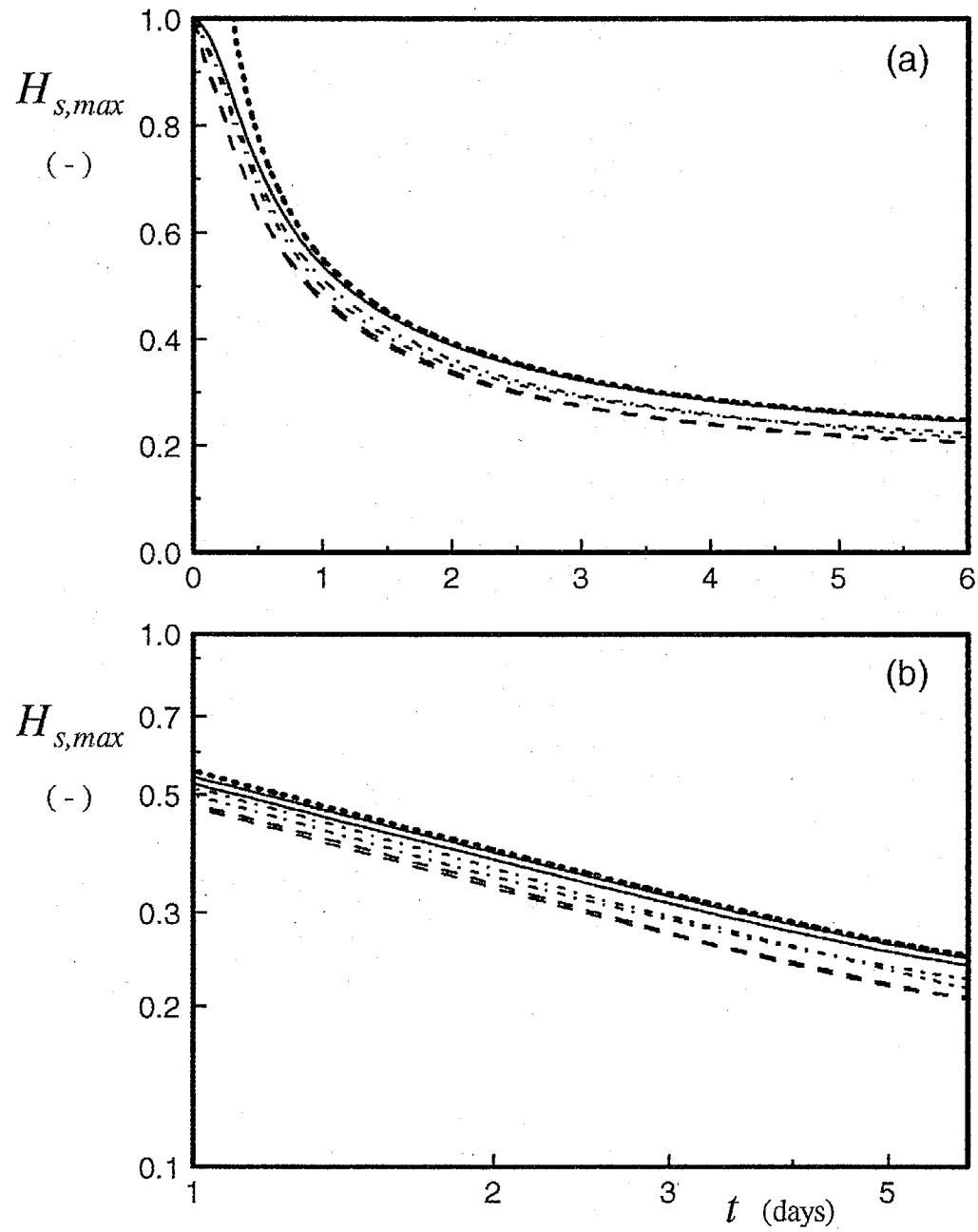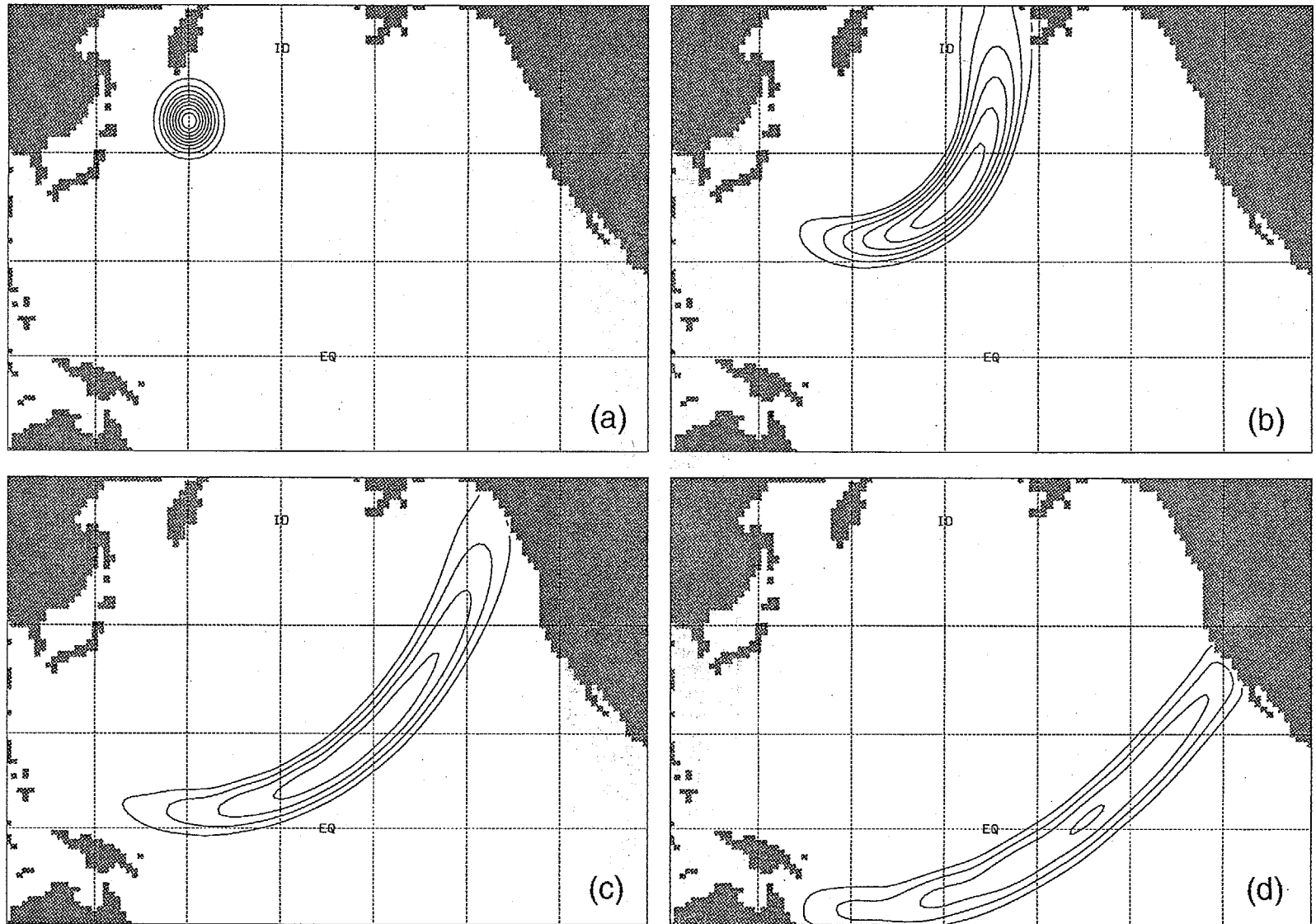
Fig. 14
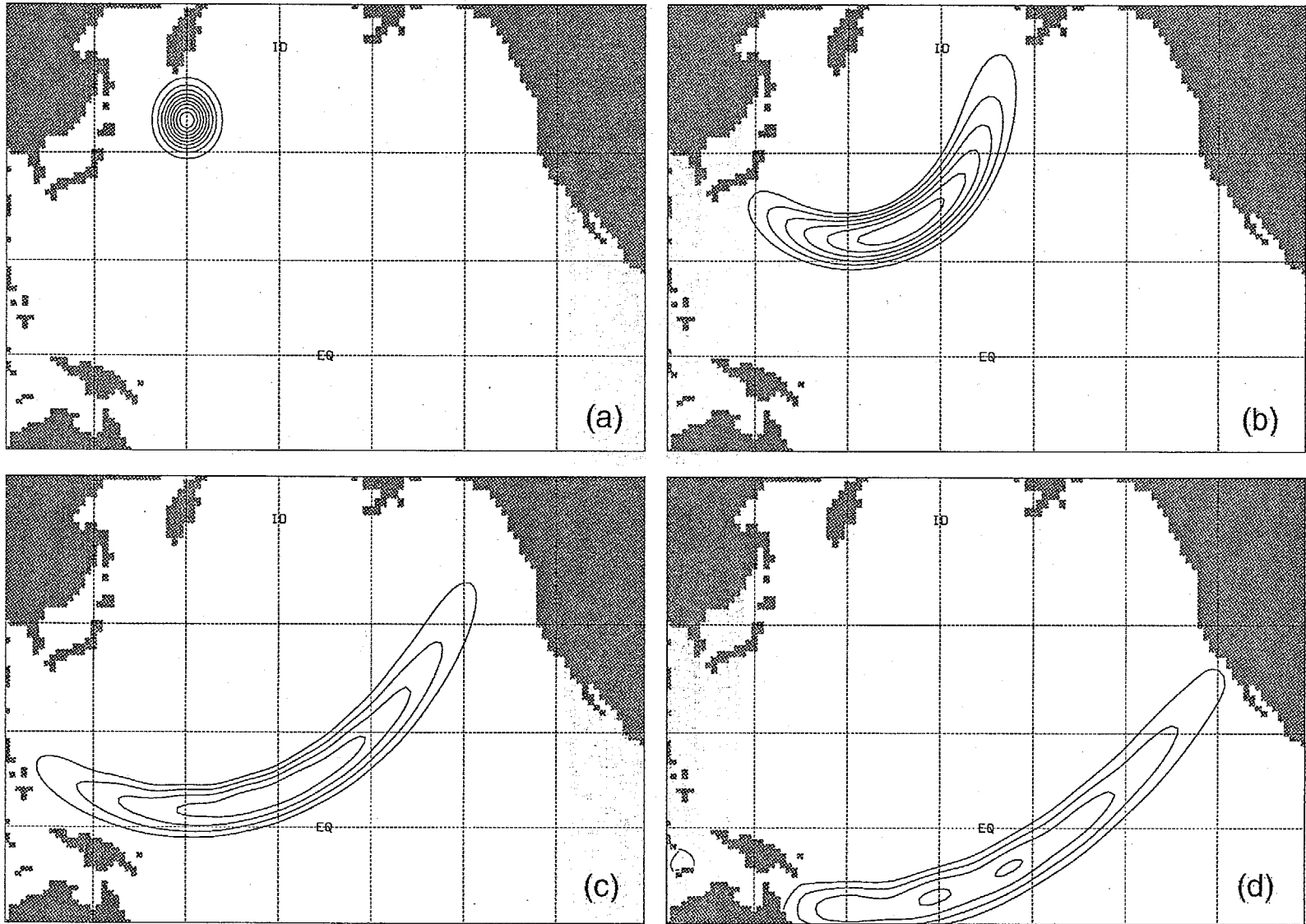
Fig. 15

Fig. 16

Fig. 17

Fig. 18

(a)

(b)

(c)

(d)
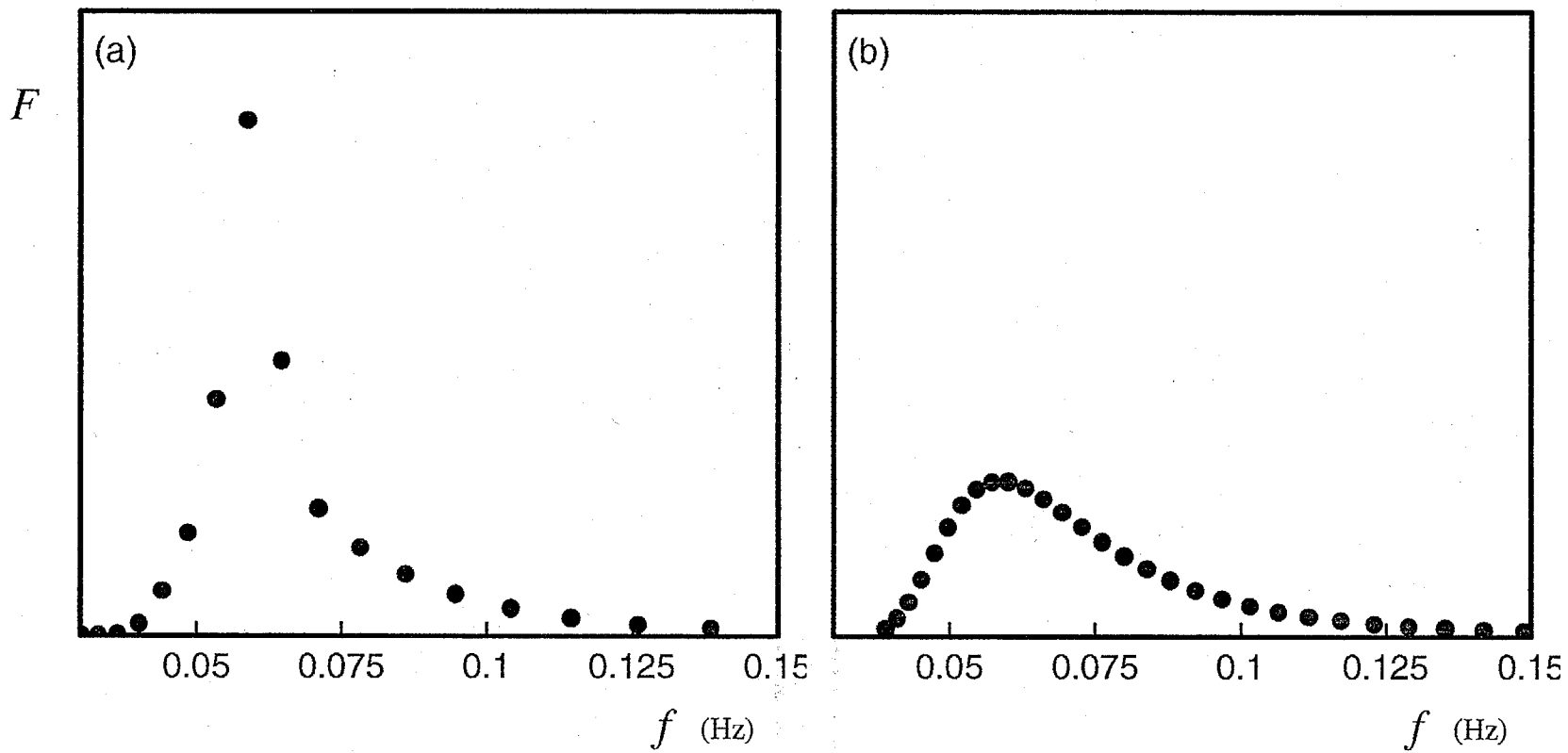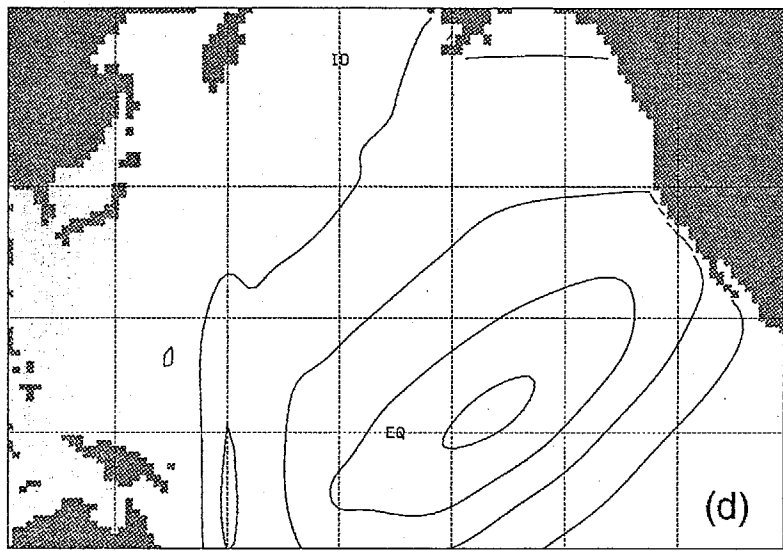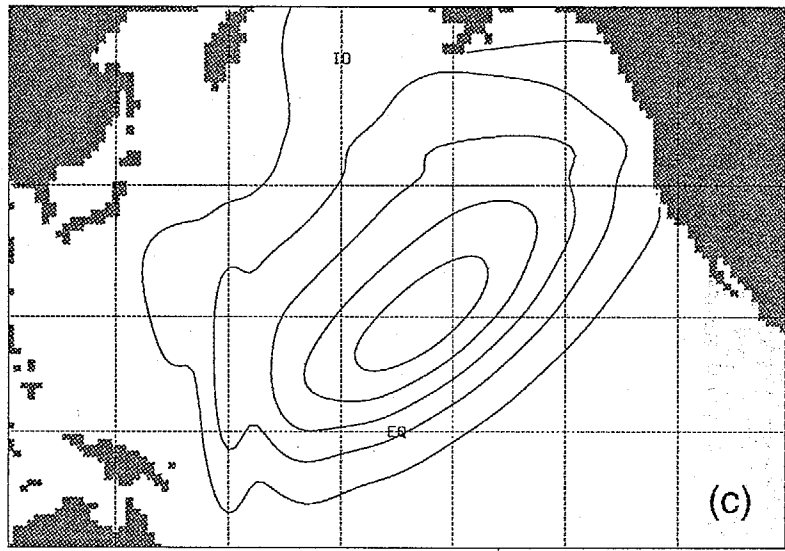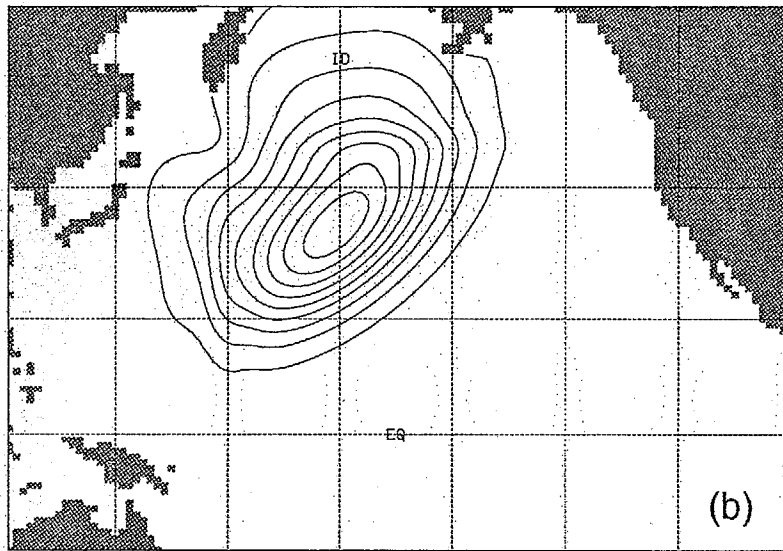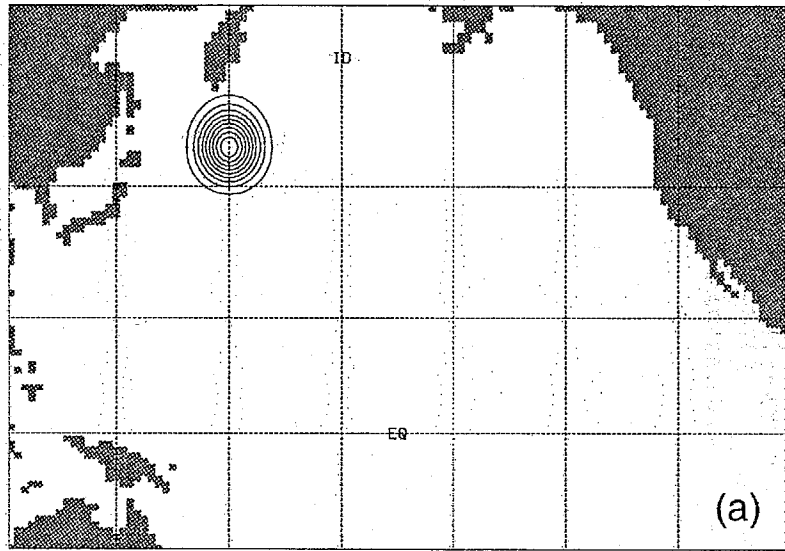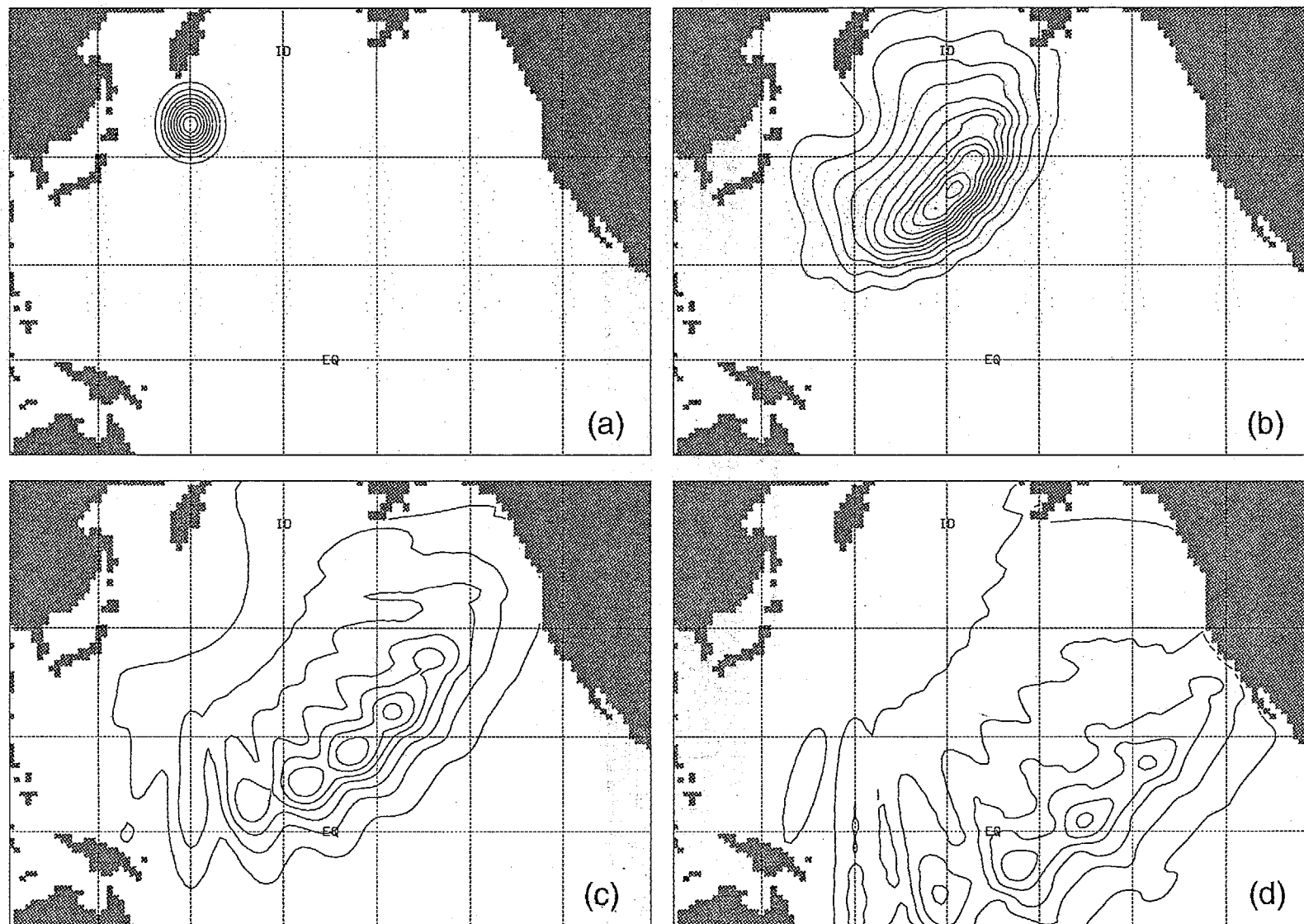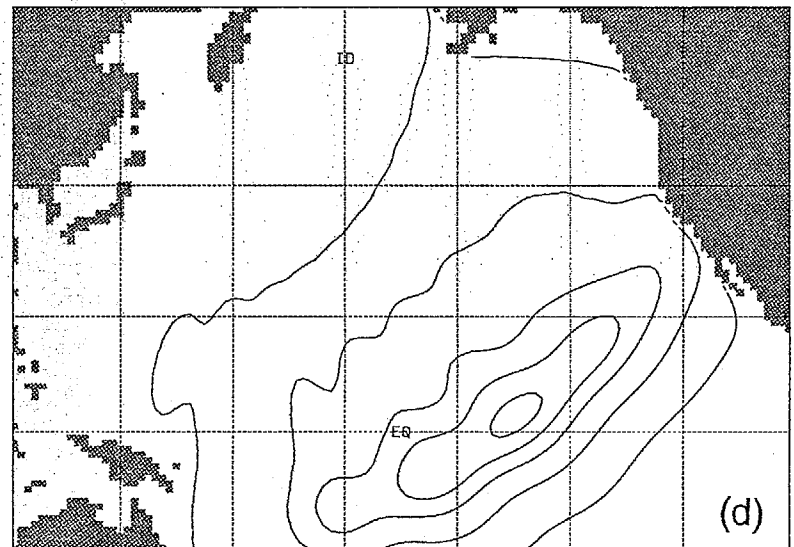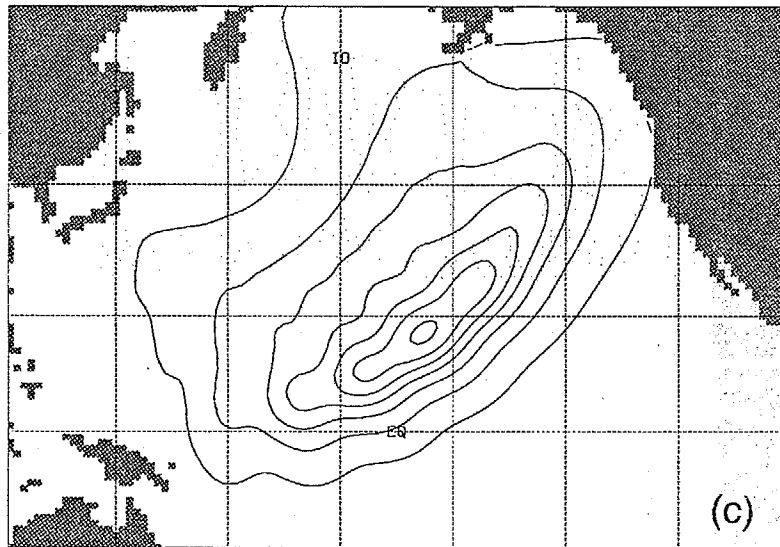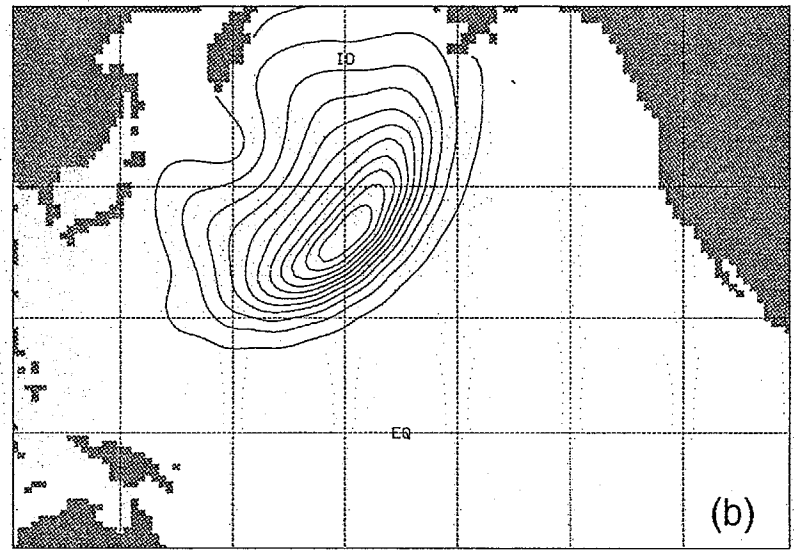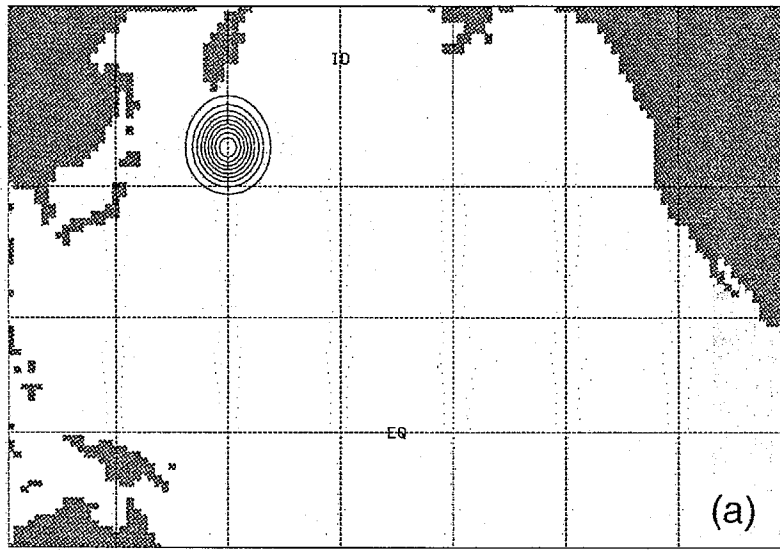
Fig. 19
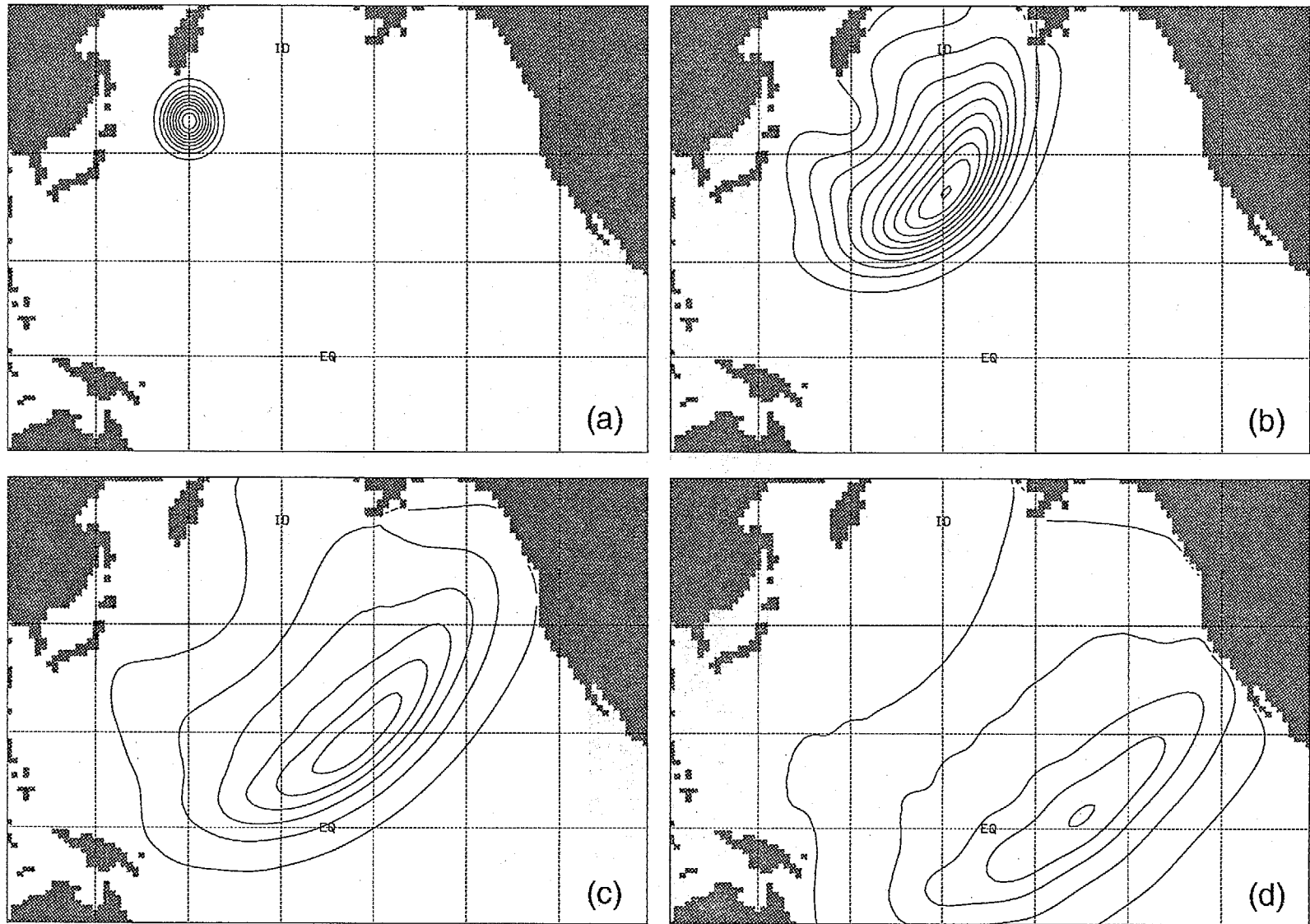
Fig. 20
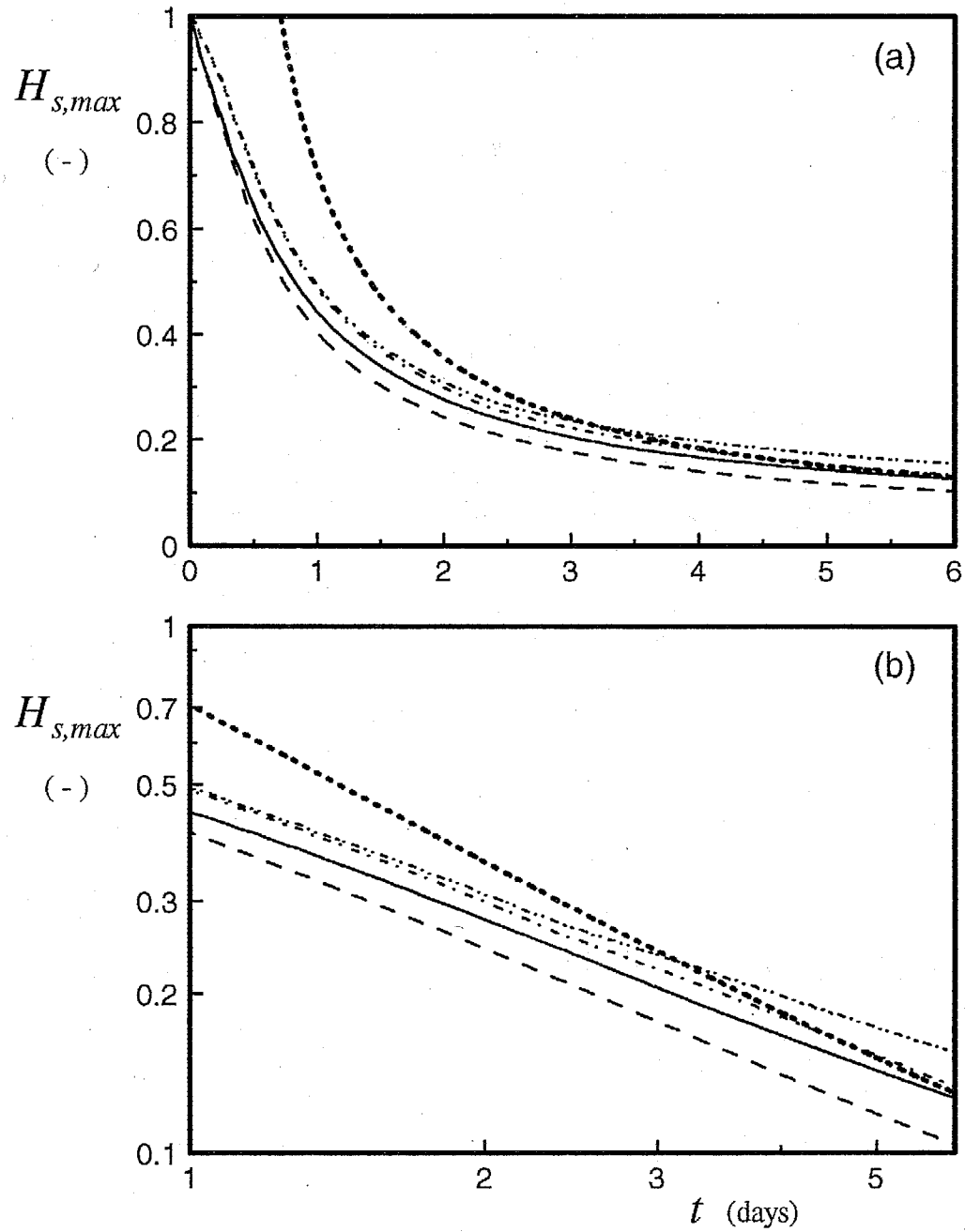
Fig. 21
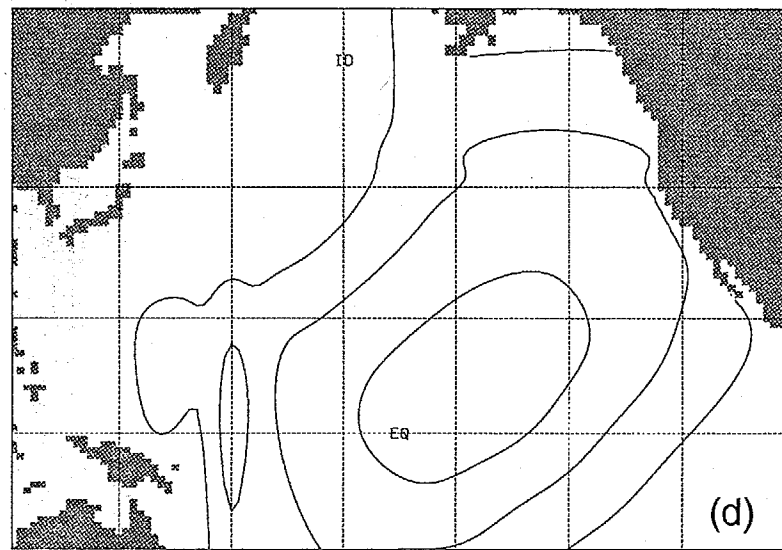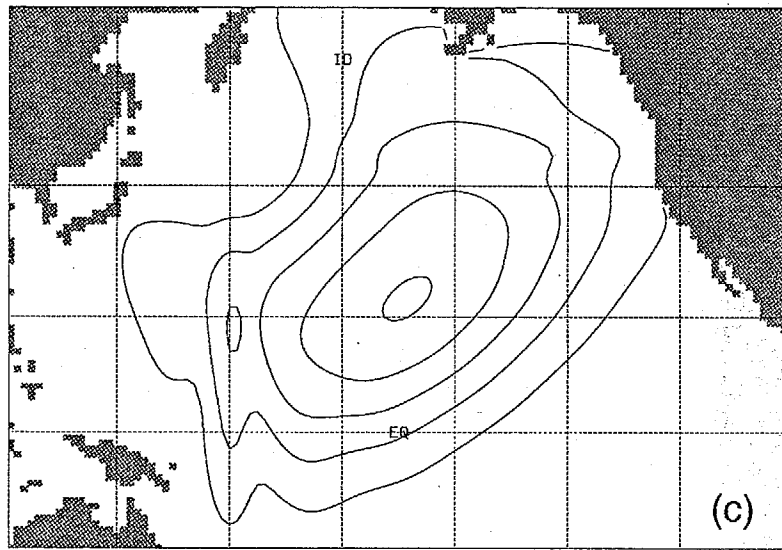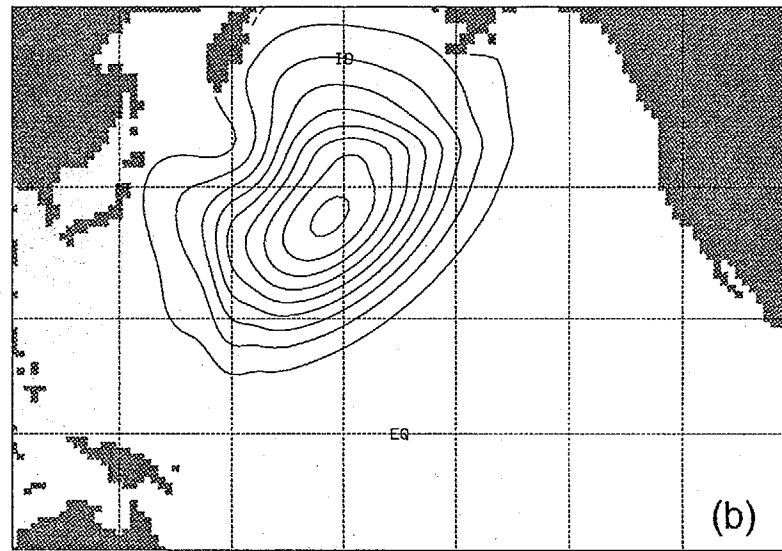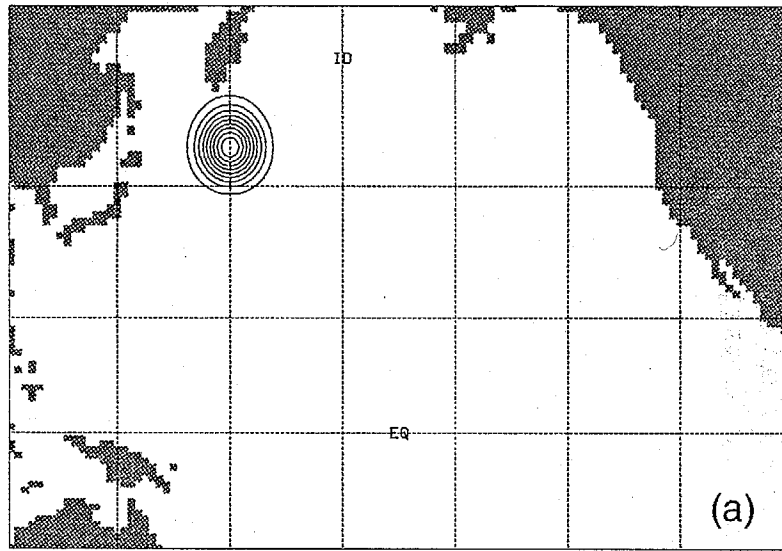
Fig. 22
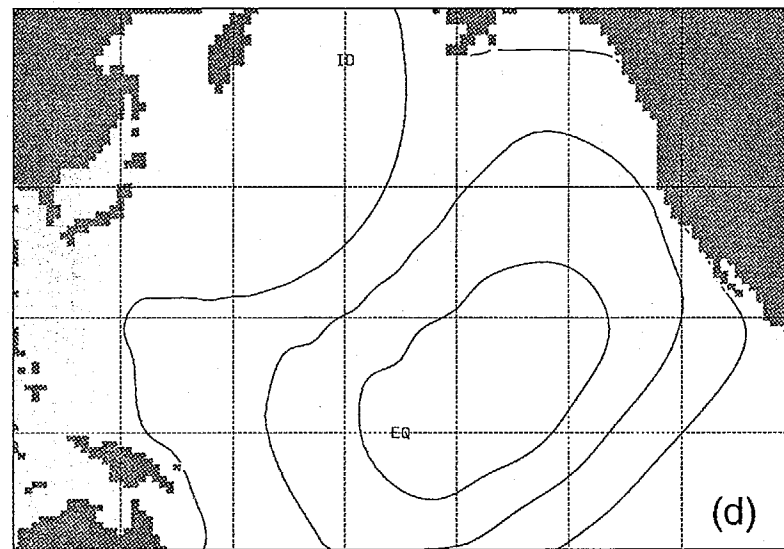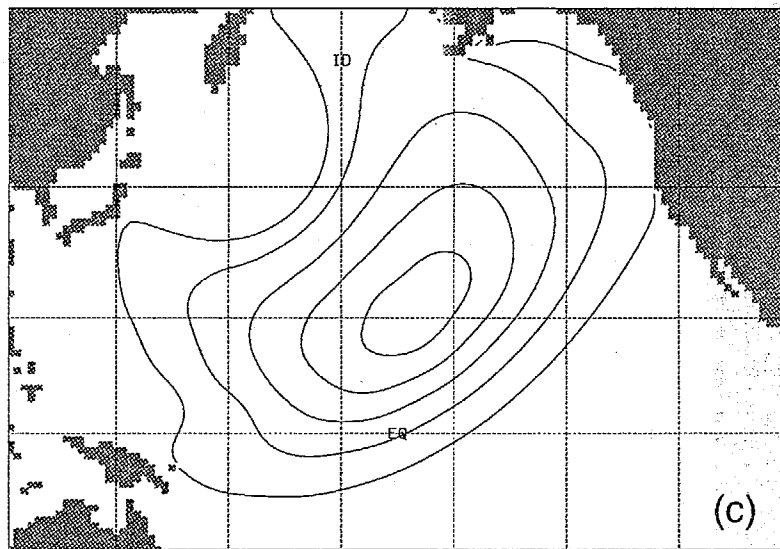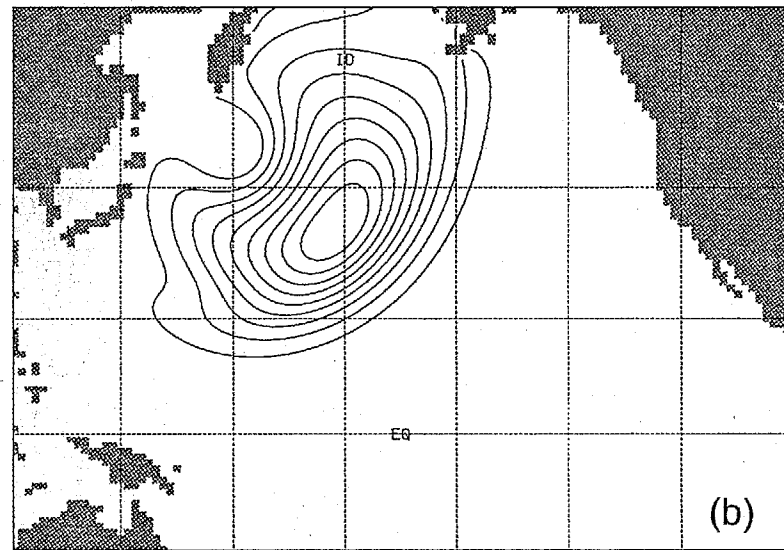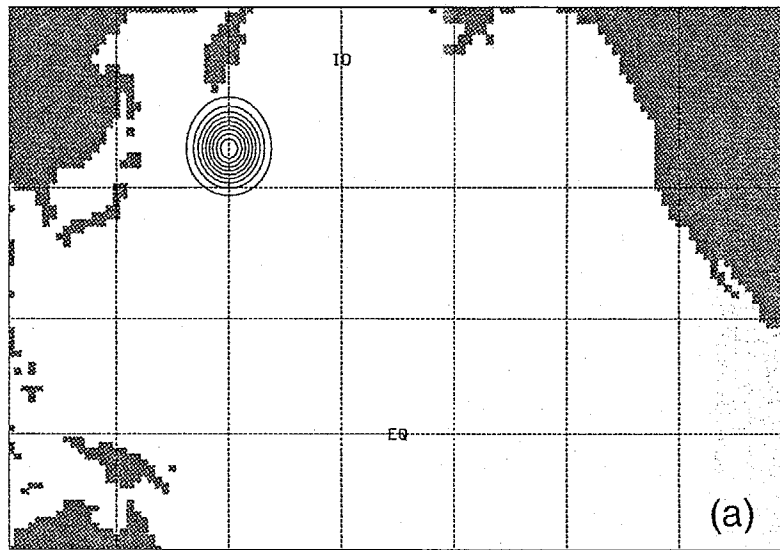
Fig. 23
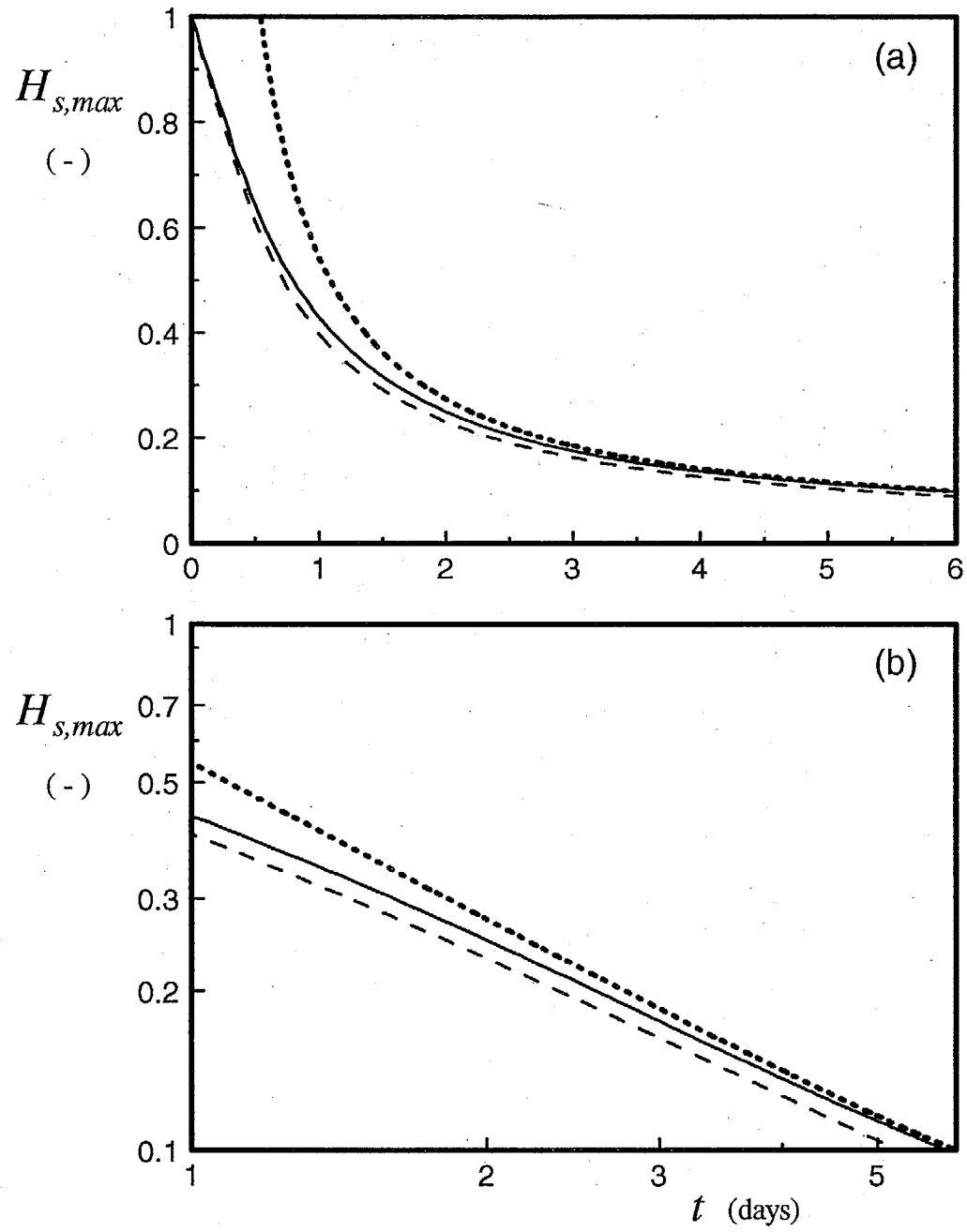
Fig. 24
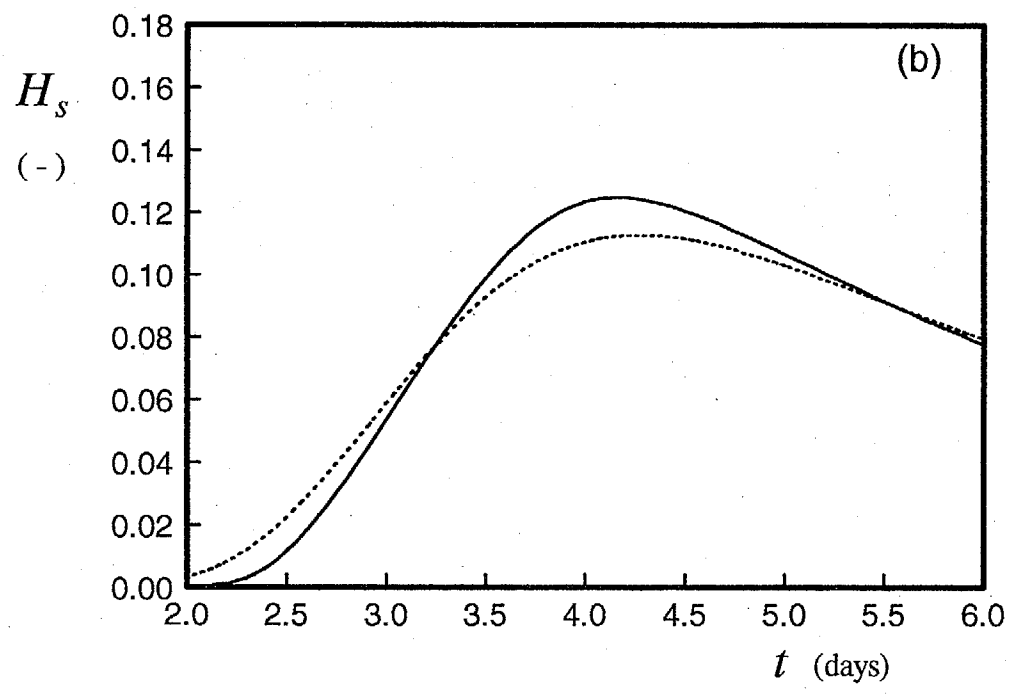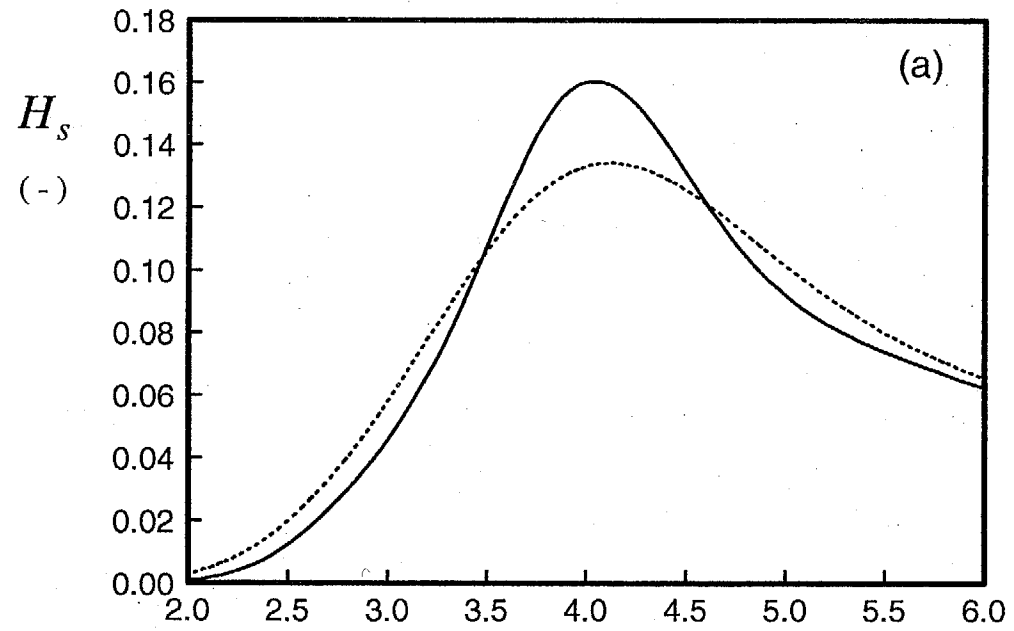
Fig. 25
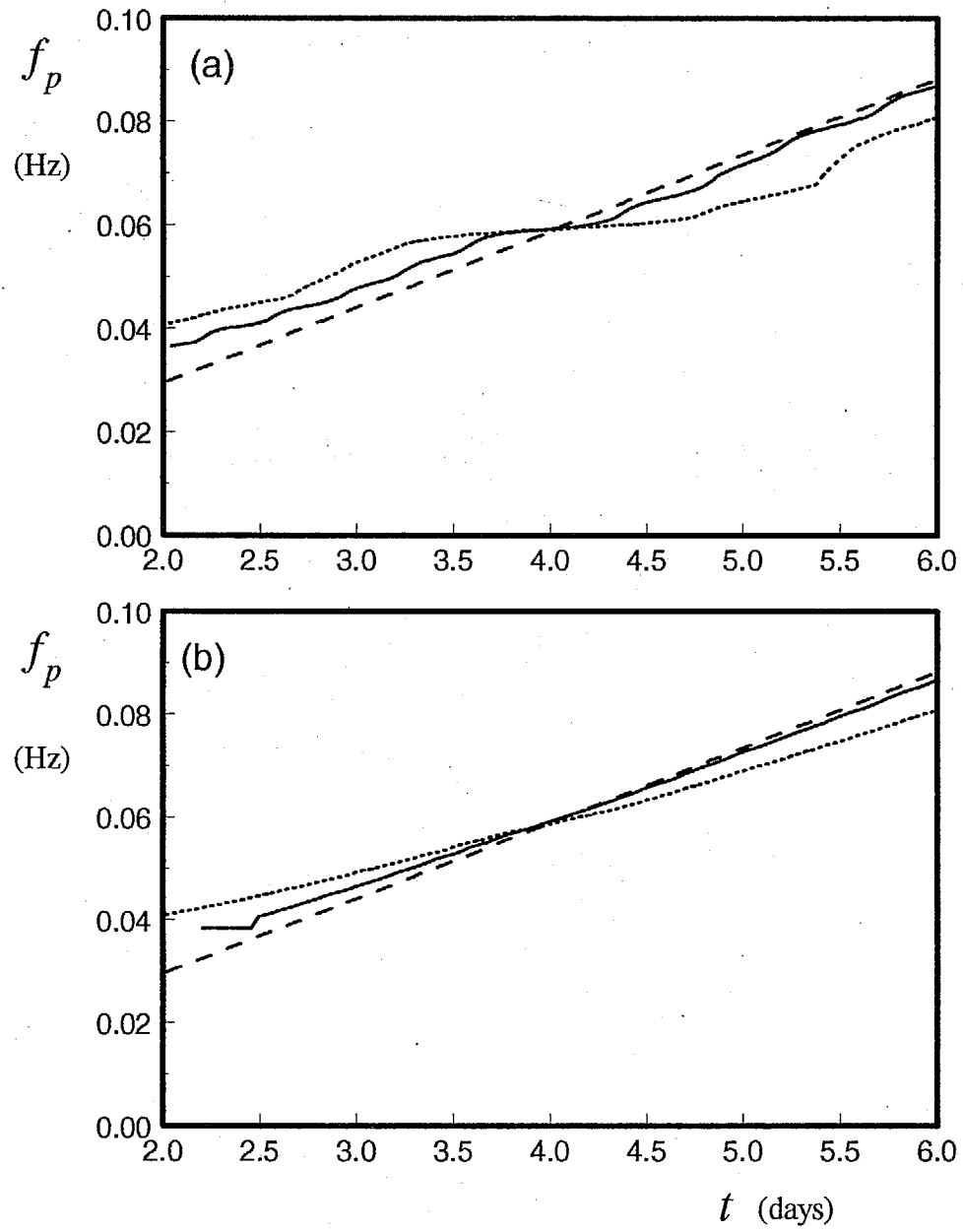
Fig. 26
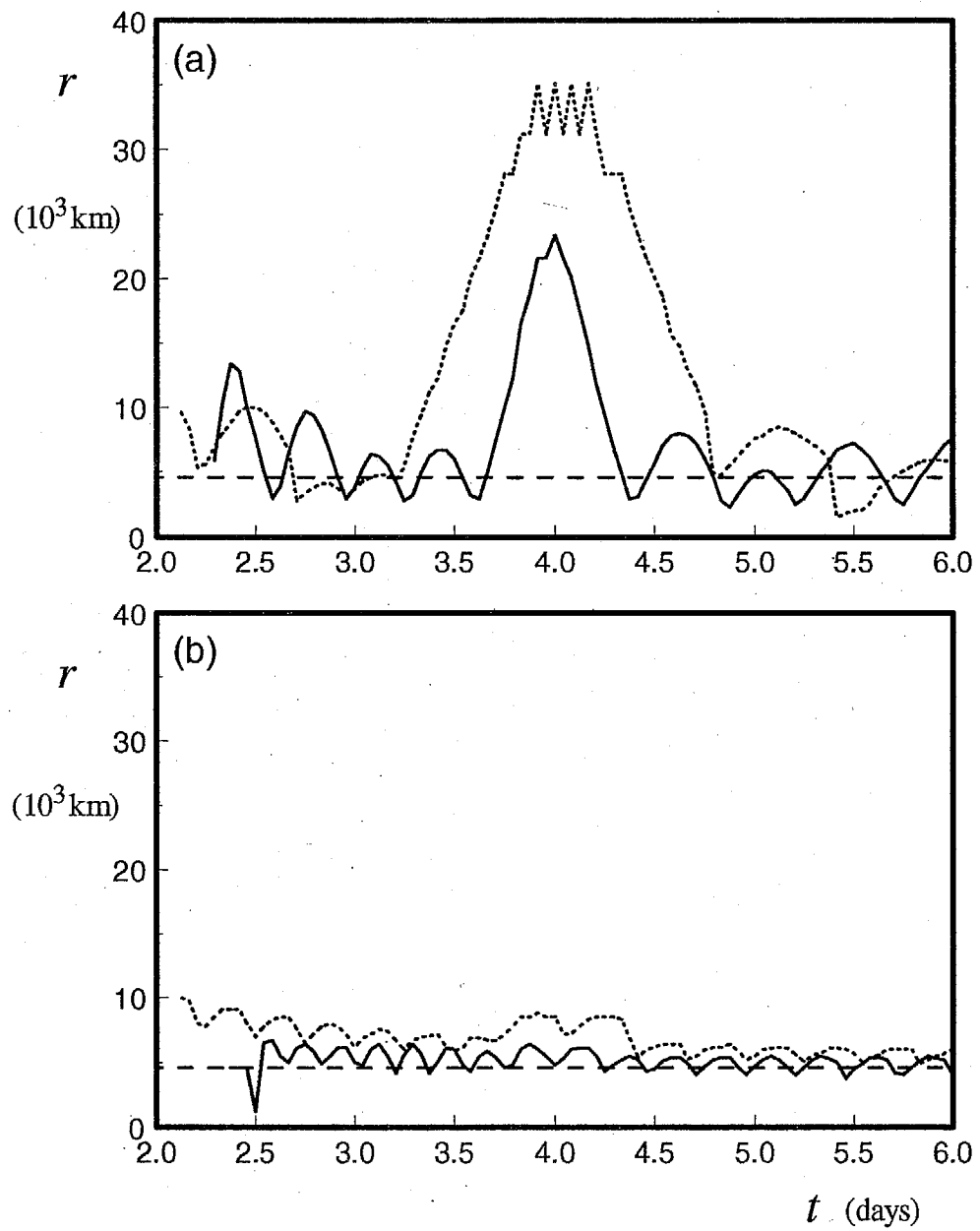
Fig. 27
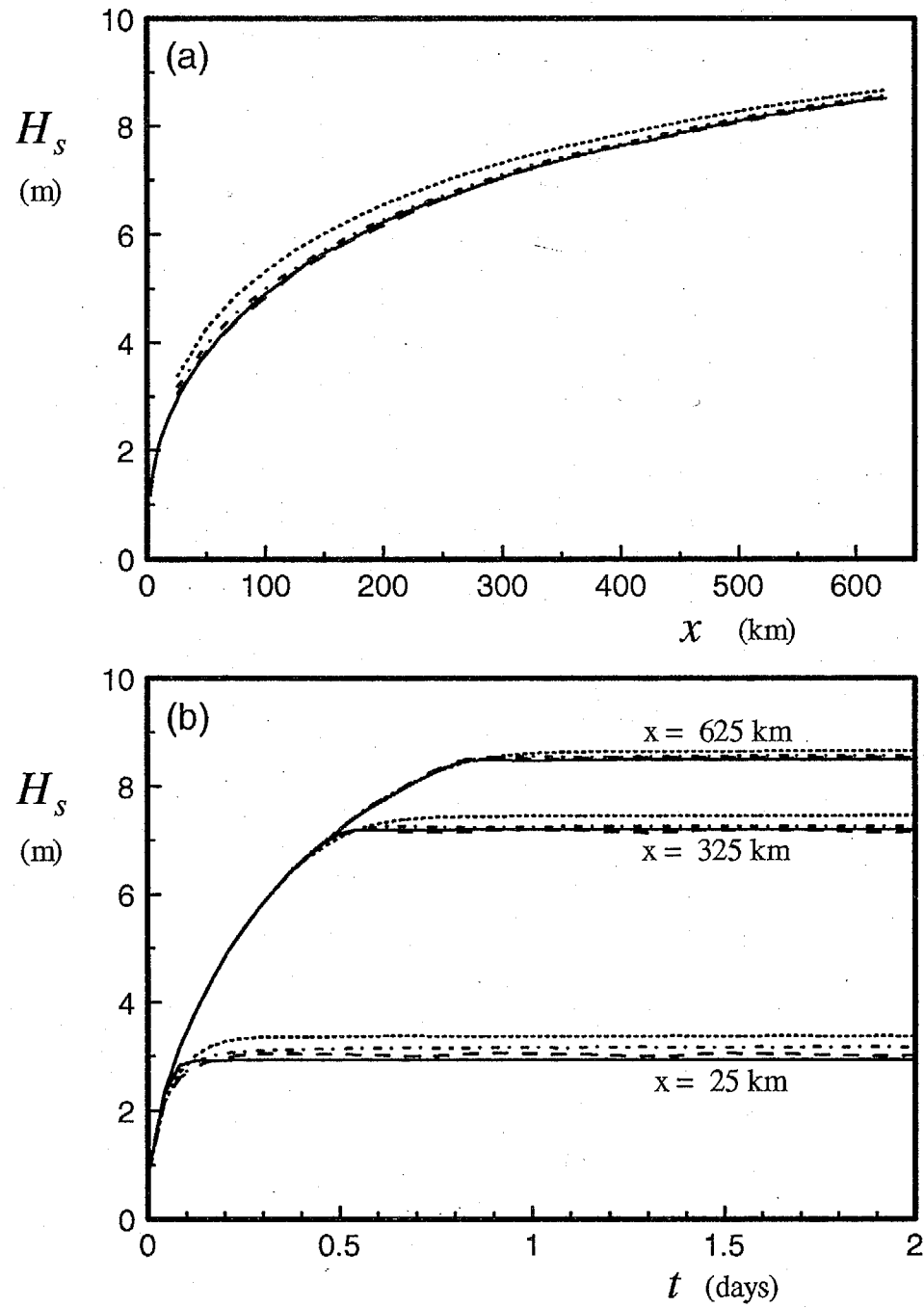
Fig. 28

OPC CONTRIBUTIONS

No. 1.   Burroughs, L. D., 1987: Development of Forecast Guidance for Santa Ana Conditions. National Weather Digest, Vol. 12 No. 1, 7pp.

No. 2.   Richardson, W. S., D. J. Schwab, Y. Y. Chao, and D. M. Wright, 1986: Lake Erie Wave Height Forecasts Generated by Empirical and Dynamical Methods -- Comparison and Verification. Technical Note, 23pp.

No. 3.   Auer, S. J., 1986: Determination of Errors in LFM Forecasts Surface Lows Over the Northwest Atlantic Ocean. Technical Note/NMC Office Note No. 313, 17pp.

No. 4.   Rao, D. B., S. D. Steenrod, and B. V. Sanchez, 1987: A Method of Calculating the Total Flow from A Given Sea Surface Topography. NASA Technical Memorandum 87799, 19pp.

No. 5.   Feit, D. M., 1986: Compendium of Marine Meteorological and Oceanographic Products of the Ocean Products Center. NOAA Technical Memorandum NWS NMC 68, 93pp.

No. 6.   Auer, S. J., 1986: A Comparison of the LFM, Spectral, and ECMWF Numerical Model Forecasts of Deepening Oceanic Cyclones During One Cool Season. Technical Note/NMC Office Note No. 312, 20pp.

No. 7.   Burroughs, L. D., 1987: Development of Open Fog Forecasting Regions. Technical Note/NMC Office Note. No. 323, 36pp.

No. 8.   Yu, T. W., 1987: A Technique of Deducing Wind Direction from Satellite Measurements of Wind Speed. Monthly Weather Review, 115, 1929-1939.

No. 9.   Auer, S. J., 1987: Five-Year Climatological Survey of the Gulf Stream System and Its Associated Rings. Journal of Geophysical Research, 92, 11,709-11,726.

No. 10. Chao, Y. Y., 1987: Forecasting Wave Conditions Affected by Currents and Bottom Topography. Technical Note, 11pp.

No. 11. Esteva, D. C., 1987: The Editing and Averaging of Altimeter Wave and Wind Data. Technical Note, 4pp.

No. 12. Feit, D. M., 1987: Forecasting Superstructure Icing for Alaskan Waters. National Weather Digest, 12, 5-10.

No. 13. Sanchez, B. V., D. B. Rao, S. D. Steenrod, 1987: Tidal Estimation in the Atlantic and Indian Oceans. Marine Geodesy, 10, 309-350.

No. 14. Gemmill, W.H., T.W. Yu, and D.M. Feit 1988: Performance of Techniques Used to Derive Ocean Surface Winds. Technical Note/NMC Office Note No. 330, 34pp.

No. 15. Gemmill, W.H., T.W. Yu, and D.M. Feit 1987: Performance Statistics of Techniques Used to Determine Ocean Surface Winds. Conference Preprint, Workshop Proceedings AES/CMOS 2nd Workshop of Operational Meteorology. Halifax, Nova Scotia, 234-243.

No. 16. Yu, T.W., 1988: A Method for Determining Equivalent Depths of the Atmospheric Boundary Layer Over the Oceans. Journal of Geophysical Research, 93, 3655-3661.

No. 17. Yu, T.W., 1987: Analysis of the Atmospheric Mixed Layer Heights Over the Oceans. Conference Preprint, Workshop Proceedings AES/CMOS 2nd Workshop of Operational Meteorology. Halifax, Nova Scotia, 2, 425-432.

No. 18. Feit, D. M., 1987: An Operational Forecast System for Superstructure Icing. Proceedings Fourth Conference Meteorology and Oceanography of the Coastal Zone, 4pp.

No. 19. Esteva, D.C., 1988: Evaluation of Priliminary Experiments Assimilating Seasat Significant Wave Height into a Spectral Wave Model. Journal of Geophysical Research, 93, 14,099-14,105.

No. 20. Chao, Y.Y., 1988: Evaluation of Wave Forecast for the Gulf of Mexico. Proceedings Fourth Conference Meteorology and Oceanography of the Coastal Zone, 42-49.

No. 21.   Breaker, L.C., 1989: El Nino and Related Variability in Sea-Surface Temperature Along the Central California Coast. PACLIM Monograph of Climate Variability of the Eastern North Pacific and Western North America, Geophysical Monograph 55, AGU, 133-140.

No. 22.   Yu, T.W., D.C. Esteva, and R.L. Teboulle, 1991: A Feasibility Study on Operational Use of Geosat Wind and Wave Data at the National Meteorological Center. Technical Note/NMC Office Note No. 380, 28pp.

No. 23.   Burroughs, L. D., 1989: Open Ocean Fog and Visibility Forecasting Guidance System. Technical Note/NMC Office Note No. 348, 18pp.

No. 24.   Gerald, V. M., 1987: Synoptic Surface Marine Data Monitoring. Technical Note/NMC Office Note No. 335, 10pp.

No. 25.   Breaker, L. C., 1989: Estimating and Removing Sensor Induced Correlation form AVHRR Data. Journal of Geophysical Reseach, 95, 9701-9711.

No. 26.   Chen, H. S., 1990: Infinite Elements for Water Wave Radiation and Scattering. International Journal for Numerical Methods in Fluids, 11, 555-569.

No. 27.   Gemmill, W.H., T.W. Yu, and D.M. Feit, 1988: A Statistical Comparison of Methods for Determining Ocean Surface Winds. Journal of Weather and Forecasting. 3, 153-160.

No. 28.   Rao. D. B., 1989: A Review of the Program of the Ocean Products Center. Weather and Forecasting. 4, 427-443.

No. 29.   Chen, H. S., 1989: Infinite Elements for Combined Diffration and Refraction . Conference Preprint, Seventh International Conference on Finite Element Methods Flow Problems, Huntsville, Alabama, 6pp.

No. 30.   Chao, Y. Y., 1989: An Operational Spectral Wave Forecasting Model for the Gulf of Mexico. Proceedings of 2nd International Workshop on Wave Forecasting and Hindcasting, 240-247.

No. 31.   Esteva, D.C., 1989: Improving Global Wave Forecasting Incorporating Altimeter Data. Proceedings of 2nd International Workshop on Wave Hindcasting and Forecasting, Vancouver, B.C., April 25-28, 1989, 378-384.

No. 32.   Richardson, W. S., J. M. Nault, D. M. Feit, 1989: Computer-Worded Marine Forecasts. Preprint, 6th Symp. on Coastal Ocean Management Coastal Zone 89, 4075-4084.

No. 33.   Chao, Y. Y., T. L. Bertucci, 1989: A Columbia River Entrance Wave Forecasting Program Developed at the Ocean Products Center. Techical Note/NMC Office Note 361.

No. 34.   Burroughs, L. D., 1989: Forecasting Open Ocean Fog and Visibility. Preprint, 11th Conference on Probability and Statisitcs, Monterey, Ca., 5pp.

No. 35.   Rao, D. B., 1990: Local and Regional Scale Wave Models. Proceeding (CMM/WMO) Technical Conference on Waves, WMO, Marine Meteorological of Related Oceanographic Activities Report No. 12, 125-138.

No. 36.   Burroughs, L.D., 1991: Forecast Guidance for Santa Ana conditions. Technical Procedures Bulletin No. 391, 11pp.

No. 37.   Burroughs, L. D., 1989: Ocean Products Center Products Review Summary. Technical Note/NMC Office Note No. 359. 29pp.

No. 38.   Feit, D. M., 1989: Compendium of Marine Meteorological and Oceanographic Products of the Ocean Products Center (revision 1). NOAA Technical Memo NWS/NMC 68.

No. 39.   Esteva, D. C., Y. Y. Chao, 1991: The NOAA Ocean Wave Model Hindcast for LEWEX. Directional Ocean Wave Spectra, Johns Hopkins University Press, 163-166.

No. 40.   Sanchez, B. V., D. B. Rao, S. D. Steenrod, 1987: Tidal Estimation in the Atlantic and Indian Oceans, 3° x 3° Solution. NASA Technical Memorandum 87812, 18pp.

No. 41.   Crosby, D.S., L.C. Breaker, and W.H. Gemmill, 1990: A Defintion for Vector Correlation and its Application to Marine Surface Winds. <u>Technical Note/NMC Office Note No. 365</u>, 52pp.

No. 42.   Feit, D.M., and W.S. Richardson, 1990: Expert System for Quality Control and Marine Forecasting Guidance. <u>Preprint, 3rd Workshop Operational and Metoerological, CMOS</u>, 6pp.

No. 43.   Gerald, V.M., 1990: OPC Unified Marine Database Verification System. <u>Technical Note/NMC Office Note No. 368</u>, 14pp.

No. 44.   Wohl, G.M., 1990: Sea Ice Edge Forecast Verification System. <u>National Weather Association Digest</u>, (submitted)

No. 45.   Feit, D.M., and J.A. Alpert, 1990: An Operational Marine Fog Prediction Model. <u>NMC Office Note No. 371</u>, 18pp.

No. 46.   Yu, T. W. , and R. L. Teboulle, 1991: Recent Assimilation and Forecast Experiments at the National Meteorological Center Using SEASAT-A Scatterometer Winds. <u>Technical Note/NMC Office Note No. 383</u>, 45pp.

No. 47.   Chao, Y.Y., 1990: On the Specification of Wind Speed Near the Sea Surface. <u>Marine Forecaster Training Manual</u>.

No. 48.   Breaker, L.C., L.D. Burroughs, T.B. Stanley, and W.B. Campbell, 1992: Estimating Surface Currents in the Slope Water Region Between 37 and 41°N Using Satellite Feature Tracking. <u>Technical Note</u>, 47pp.

No. 49.   Chao, Y.Y., 1990: The Gulf of Mexico Spectral Wave Forecast Model and Products. <u>Technical Procedures Bulletin No. 381</u>, 3pp.

No. 50.   Chen, H.S., 1990: Wave Calculation Using WAM Model and NMC Wind. <u>Preprint, 8th ASCE Engineering Mechanical Conference, 1</u>, 368-372.

No. 51.   Chao, Y.Y., 1990: On the Transformation of Wave Spectra by Current and Bathymetry. <u>Preprint, 8th ASCE Engineering Mechnical Conference, 1</u>, 333-337.

No. 52.   WAS NOT PUBLISHED

No. 53.   Rao, D.B., 1991: Dynamical and Statistical Prediction of Marine Guidance Products. <u>Proceedings, IEEE Conference Oceans 91</u>, 3, 1177-1180.

No. 54.   Gemmill, W.H., 1991: High-Resolution Regional Ocean Surface Wind Fields. <u>Proceedings, AMS 9th Conference on Numerical Weather Prediction</u>, Denver, CO, Oct. 14-18, 1991, 190-191.

No. 55.   Yu, T.W., and D. Deaven, 1991: Use of SSM/I Wind Speed Data in NMC's GDAS. <u>Proceedings, AMS 9th Conference on Numerical Weather Prediction</u>, Denver, CO, Oct. 14-18, 1991, 416-417.

No. 56.   Burroughs, L.D., and J.A. Alpert, 1993: Numerical Fog and Visiability Guidance in Coastal Regions. <u>Technical Procedures Bulletin. No. 398</u>, 6pp.

No. 57.   Chen, H.S., 1992: Taylor-Gelerkin Method for Wind Wave Propagation. <u>ASCE 9th Conf. Eng. Mech.</u> (in press)

No. 58.   Breaker, L.C., and W.H. Gemmill, and D.S. Crosby, 1992: A Technique for Vector Correlation and its Application to Marine Surface Winds. <u>AMS 12th Conference on Probability and Statistics in the Atmospheric Sciences</u>, Toronto, Ontario, Canada, June 22-26, 1992.

No. 59.   Yan, X.-H. and Breaker, L.C., 1993: Surface Circulation Estimation Using Image Processing and Computer Vision Methods Applied to Sequential Satellite Imagery. Photogrammetric Engineering and Remote Sensing, 59, 407-413.

No. 60.   Wohl, G., 1992: Operational Demonstration of ERS-1 SAR Imagery at the Joint Ice Center. <u>Proceeding of the MTS 92 - Global Ocean Partnership</u>, Washington, DC, Oct. 19-21, 1992.

No. 61.   Waters, M.P., Caruso, W.H. Gemmill, W.S. Richardson, and W.G. Pichel, 1992: An Interactive Information and Processing System for the Real-Time Quality Control of Marine Meteorological Oceanographic Data. Pre-print 9th International Conference on Interactive Information and Processing System for Meteorology, Oceanography and Hydrology, Anaheim, CA, Jan. 17-22, 1993.

No. 62.   Breaker, L.C., and V. Krasnopolsky, 1994: The Problem of AVHRR Image Navigation Revisited. Int. Journal of Remote Sensing, 15, 979-1008.

No. 63.   Crosby, D.S., L.C. Breaker, and W.H. Gemmill, 1993: A Proposed Definition for Vector Correlation in Geophysics: Theory and Application. Journal of Atmospheric and Ocean Technology, 10, 355-367.

No. 64.   Grumbine, R., 1993: The Thermodynamic Predictability of Sea Ice. Journal of Glaciology, 40, 277-282, 1994.

No. 65.   Chen, H.S., 1993: Global Wave Prediction Using the WAM Model and NMC Winds. 1993 International Conference on Hydro Science and Engineering, Washington, DC, June 7 - 11, 1993. (submitted)

No. 66.   WAS NOT PUBLISHED

No. 67.   Breaker, L.C., and Alan Bratkovich, 1993: Coastal-Ocean Processes and their Influence on the Oil Spilled off San Francisco by the M/V Puerto Rican. Marine Environmental Research, 36, 153-184.

No. 68.   Breaker, L.C., L.D. Burroughs, J.F. Culp, N.L. Gunasso, R. Teboulle, and C.R. Wong, 1993: Surface and Near-Surface Marine Observations During Hurricane Andrew. Technical Notes/NMC Office Note #398, 41pp.

No. 69.   Burroughs, L.D., and R. Nichols, 1993: The National Marine Verification Program - Concepts and Data Management, Technical Note/NMC Office Note #393, 21pp.

No. 70.   Gemmill, W.H., and R. Teboulle, 1993: The Operational Use of SSM/I Wind Speed Data over Oceans. Pre-print 13th Conference on Weather Analyses and Forecasting, AMS Vienna, VA., August 2-6, 1993, 237-238.

No. 71.   Yu, T.-W., J.C. Derber, and R.N. Hoffman, 1993: Use of ERS-1 Scatterometer Backscattered Measurements in Atmospheric Analyses. Pre-print 13th Conference on Weather Analyses and Forecasting, AMS, Vienna, VA., August 2-6, 1993, 294-297.

No. 72.   Chalikov, D. and Y. Liberman, 1993: Director Modeling of Nonlinear Waves Dynamics. J. Physical, (To be submitted).

No. 73.   Woiceshyn, P., T.W. Yu, W.H. Gemmill, 1993: Use of ERS-1 Scatterometer Data to Derive Ocean Surface Winds at NMC. Pre-print 13th Conference on Weather Analyses and Forecasting, AMS, Vienna, VA, August 2-6, 1993, 239-240.

No. 74.   Grumbine, R.W., 1993: Sea Ice Prediction Physics. Technical Note/NMC Office Note #396, 44pp.

No. 75.   Chalikov, D., 1993: The Parameterization of the Wave Boundary Layer. Journal of Physical Oceanography, Vol. 25, No. 6, Par 1, 1333-1349.

No. 76.   Tolman, H.L., 1993: Modeling Bottom Friction in Wind-Wave Models. Ocean Wave Measurement and Analysis, O.T. Magoon and J.M. Hemsley Eds., ASCE, 769-783.

No. 77.   Breaker, L., W. Broenkow, 1994: The Circulation of Monterey Bay and Related Processes. Oceanography and Marine Biology: An Annual Review, 32, 1-64.

No. 78.   Chalikov, D., D. Esteva, M. Iredell and P. Long, 1993: Dynamic Coupling between the NMC Global Atmosphere and Spectral Wave Models. Technical Note/NMC Office Note #395, 62pp.

No. 79.   Burroughs, L.D., 1993: National Marine Verification Program - Verification Statistics - Verification Statistics, Technical Note/NMC Office Note #400, 49 pp.

No. 80.   Shashy, A.R., H.G. McRandal, J. Kinnard, and W.S. Richardson, 1993: Marine Forecast Guidance from an Interactive Processing System. 74th AMS Annual Meeting, January 23 - 28, 1994.

No. 81.   Chao, Y.Y., 1993: The Time Dependent Ray Method for Calculation of Wave Transformation on Water of Varying Depth and Current. Wave 93 ASCE.

No. 82.   Tolman, H.L., 1994: Wind-Waves and Moveable-Bed Bottom Friction. Journal of Physical Oceanography, 24, 994-1009.

No. 83.   Grumbine, R.W., 1993: Notes and Correspondence A Sea Ice Albedo Experiment with the NMC Meduim Range Forecast Model. Weather and Forecasting, (submitted).

No. 84.   Chao, Y.Y., 1993: The Gulf of Alaska Regional Wave Model. Technical Procedure Bulletin, No. 427, 10 pp.

No. 85.   Chao, Y.Y., 1993: Implementation and Evaluation of the Gulf of Alaska Regional Wave Model. OPC Office Note, 35 pp.

No. 86.   WAS NOT PUBLISHED.

No. 87.   Burroughs, L., 1994: Portfolio of Operational and Development Marine Meteorological and Oceanographic Products. NCEP Office Note. In preparation.

No. 88.   Tolman, H.L., D. Chalikov, 1994: Development of a third-generation ocena wave model at NOAA-NMC. Proc. Waves Physical and Numberial Modelling, M. Isaacson and M.C. Quick Eds., Vancouver, 724-733.

No. 89.   Peters, C., W. Gemmill, V. Gerald, and P. Woiceshyn, 1994: Evaluation of Empirical Transfer Functions for ERS-1 Scatterometer Data at NMC. 7th Conference on Satellite Meteorology and Oceanography, June 6-10, 1994, Monterey, CA., pg. 550-552.

No. 90.   Breaker, L.C., and C.R.N. Rao, 1996: The Effects of Aerosols from the Mt. Pinatubo and Mt. Hudson Volcanio Eruption on Satellite-Derived Sea Surface Temperatures. Journal of Geophysical Research. (To be submitted).

No. 91.   Yu, W., P. Woiceshyn, W. Gemmill, and C. Peters, 1994: Analysis & Forecast Experiments at NMC Using ERS-1 Scatterometer Wind Measurements. 7th Conference on Satellite Meteorology and Oceanography, June 6-10, 1994, Monterey, CA., pg. 600-601.

No. 92.   Chen, H.S., 1994: Ocean Surface Waves. Technical Procedures Bulletin, No. 426, 17 pp.

No. 93.   Breaker, L.C., V. Krasnopolsky, D.B. Rao, X.-H. Yan, 1994: The Feasibility of Estimating Ocean Surface Currents on an Operational Basis using Satellite Feature Tracking Methods. Bulletin of the American Meteorolgical Society, 75, 2085-2095.

No. 94.   Krasnopolsky, L. Breaker, and W. Gemmill, 1994: Development of Single "All-Weather" Neural Network Algorithms for Estimating Ocean Surface Winds from the Special Sensor Microwave Imager. NMC, OPC Contribution Note.

No. 95.   Breaker, L.C., D.S. Crosby and W.H. Gemmill, 1994: The application of a New Definition for Vector Correlation to Problems in Oceanography and Meteorology. Journal of Applied Meteolorology, 33, 1354-1365.

No. 96.   Peters, C.A., V.M. Gerald, P.M. Woiceshyn, W.H. Gemmill, 1994: Operational Processing of ERS-1 Scatterometer winds: A Documentation. OPC Office Note.

No. 97.   Gemmill, G., P. Woiceshyn, C. Peters, and V. Gerald, 1994: A Preliminary Evaluation Scatterometer Wind Transfer Functions for ERS-1 Data. OPC Office Note.

No. 98.   Chen, H.S., 1994: Evaluation of a Global Ocean Wave Model at NMC. International Conference on Hydro-Science and Engineering. Beijing, China, March 22 - 26, 1995.

No. 99.   Aikman, F. and D.B. Rao, 1994: NOAA Perspective on a Coastal Forecast System.

No. 100.   Rao, D.B. and C. Peters, 1994: Two-Dimensional Co-Oscillations in a Rectangular Bay: Possible Application to Water
               Problems. OPC Office Note.

No. 101   Breaker, L.C., L.D. Burroughs, Y.Y. Chao, J.F. Culp, N.L. Gunasso, R. Teboulle, and C.R. Wong, 1994: Surface and Near-
               Surface Marine Observations During Hurricane Andrew. Weather and Forecasting, 9, 542-556.

No. 102   Tolman, H.L., 1995: Subgrid Modeling of Moveable-bed Bottom Friction in Wind Wave Models. Coastal Engineering, (in
               press).

No. 103   Breaker, L.C., D.B. Gilhousen, H.L. Tolman and L.D. Burroughs, 1995: Initial Results from Long-Term Measurements of
               Atmospheric Humidity and Related Parameters the Marine Boundary Layer at Two Locations in the Gulf of Mexico. (To be
               submitted to Global Atmosphere and Ocean Systems.

No. 104   Burroughs, L.D., J.P. Dallavalle, 1995: Great Lakes Wind and Wave Guidance. Technical Procedures Bulletin No., (In
               preparation).

No. 105   Burroughs, L.D., J.P. Dallavalle, 1995: Great Lakes Storm Surge Guidance. Technical Procedures Bulletin No., (In
               preparation).

No. 106   Shaffer, W.A., J.P. Dallavalle, and L.D. Burroughs, 1995: East Coast Extratropical Storm Surge and Beach Erosion
               Guidance. Technical Procedures Bulletin No., (In preparation)

No. 107   WAS NOT PUBLISHED.

No. 108   WAS NOT PUBLISHED.

No. 109   WAS NOT PUBLISHED.

No. 110   Gemmill, W.H, and C.A. Peters, 1995: The Use of Satellite Dervired Wind Data in High-Resolution Regional Ocean
               Surface Wind Fields. Conf. on Coastal Oceanic and Atmospheric Prediction, Jan 28 - Feb 2, 1996, Atlanta, GA (acceptec
               did at preprint press).

OPC CHANGES TO OMB

No. 111   Krasnopolsky, V.M, W.H. Gemmill, L.C. Breaker, 1995: Improved SSM/I Wind Speed Retrievals at Higher Wind Speeds.
               Journal of Geophysical Research, (in press).

No. 112   Chalikov, D, L.D. Breaker, and L. Lobocki, 1995: A Simple Model of Mixing in the Upper Ocean. Journal of Physical
               Ocean, (in press).

No. 113   Tolman, H.L., 1995: On the Selection of Propagation Schemes for a Spectral Wind-Wave Model, OMB Office Note.